Molecular Therapy
Original Article

WNT-modulating gene silencers as a gene therapy for osteoporosis, bone fracture, and critical-sized bone defects

Won-Taek Oh,[1,2,11] Yeon-Suk Yang,[1,11] Jun Xie,[3,4,5] Hong Ma,[3,4,5] Jung-Min Kim,[1] Kwang-Hwan Park,[2] Daniel S. Oh,[6] Kyung-Hyun Park-Min,[7,8] Matthew B. Greenblatt,[8,9] Guangping Gao,[3,4,5,10] and Jae-Hyuck Shim[1,3,10]

[1]Department of Medicine, Division of Rheumatology, University of Massachusetts Chan Medical School, 364 Plantation Street. LRB 217, Worcester, MA 01605, USA; [2]Department of Orthopedic Surgery, Yonsei University College of Medicine, Seoul 03722, Korea; [3]Horae Gene Therapy Center, University of Massachusetts Chan Medical School, 368 Plantation Street AS6-2049, Worcester, MA 01605, USA; [4]Department of Microbiology and Physiological Systems, University of Massachusetts Chan Medical School, 368 Plantation Street AS6-2049, Worcester, MA 01605, USA; [5]Viral Vector Core, University of Massachusetts Chan Medical School, 368 Plantation Street AS6-2049, Worcester, MA 01605, USA; [6]Osteogene Tech, Norwood, NJ 07648, USA; [7]Arthritis and Tissue Degeneration Program, David Z. Rosensweig Genomics Research Center, Hospital for Special Surgery, New York, NY 10021, USA; [8]Research Division, Hospital for Special Surgery, New York, NY 10021, USA; [9]Department of Pathology and Laboratory Medicine, Weill Cornell Medical College, New York, NY 10021, USA; [10]Li Weibo Institute for Rare Diseases Research, University of Massachusetts Chan Medical School, 368 Plantation Street AS6-2049, Worcester, MA 01605, USA

Treating osteoporosis and associated bone fractures remains challenging for drug development in part due to potential off-target side effects and the requirement for long-term treatment. Here, we identify recombinant adeno-associated virus (rAAV)-mediated gene therapy as a complementary approach to existing osteoporosis therapies, offering long-lasting targeting of multiple targets and/or previously undruggable intracellular non-enzymatic targets. Treatment with a bone-targeted rAAV carrying artificial microRNAs (miRNAs) silenced the expression of WNT antagonists, schnurri-3 (SHN3), and sclerostin (SOST), and enhanced WNT/β-catenin signaling, osteoblast function, and bone formation. A single systemic administration of rAAVs effectively reversed bone loss in both postmenopausal and senile osteoporosis. Moreover, the healing of bone fracture and critical-sized bone defects was also markedly improved by systemic injection or transplantation of AAV-bound allograft bone to the osteotomy sites. Collectively, our data demonstrate the clinical potential of bone-specific gene silencers to treat skeletal disorders of low bone mass and impaired fracture repair.

INTRODUCTION

Skeletal remodeling is a process of continuous bone replacement regulated by interactions between bone-forming osteoblasts and bone-resorbing osteoclasts, and remodeling is crucial for maintaining bone quality and proper fracture healing.[1] Current osteoporosis drugs that inhibit osteoclast-mediated bone resorption have been reported to impair bone remodeling after long-term treatment. These antiresorptive drugs have also been reported to impair bone formation in the setting of a bone fracture or a critical-sized bone defect, which makes anabolic agents attractive for these indications.[2-5] Two anabolic agents, intermittent parathyroid hormone (PTH) and PTH-related protein (PTHrP), are also available to treat patients with osteoporosis, but the anabolic activity of PTH is counterbalanced by increased osteoclast activity. Additionally, these agents are limited in their total duration of use based on oncogenic effects observed with markedly supratherapeutic doses in rodent trials.[6-8] Since the WNT pathway is a pivotal regulator of bone formation that mediates the augmentation of bone quantity and the maintenance of bone remodeling,[9] WNT signaling components, such as sclerostin (SOST) and schnurri-3 (SHN3, also *Hivep3*), have been considered promising targets to promote bone formation in osteoporosis and fracture healing.

SOST is a secreted antagonist of WNT signaling that interferes with the interaction between WNTs and their cognate receptor Frizzled by binding to the WNT co-receptors low-density lipoprotein receptor-related proteins 5 and 6 (LRP5/6; Figure S1).[10] A humanized monoclonal anti-SOST antibody significantly increased bone mineral density along with elevated levels of bone-formation markers over the first 6 to 9 months of treatment in postmenopausal women.[11] However, treatment for more than 1 year is not recommended because the bone-forming response wanes over time, as

Received 24 May 2022; accepted 28 September 2022;
https://doi.org/10.1016/j.ymthe.2022.09.018.

[11]These authors contributed equally

Correspondence: Guangping Gao, PhD, Horae Gene Therapy Center, Li Weibo Institute for Rare Diseases Research, University of Massachusetts Chan Medical School, 368 Plantation Street AS6-2049, Worcester, MA 01605, USA.
E-mail: guangping.gao@umassmed.edu
Correspondence: Jae-Hyuck Shim, PhD, Department of Medicine, Division of Rheumatology, Horae Gene Therapy Center, Li Weibo Institute for Rare Diseases Research, University of Massachusetts Chan Medical School, 364 Plantation Street. LRB 217, Worcester, MA 01605, USA.
E-mail: jaehyuck.shim@umassmed.edu

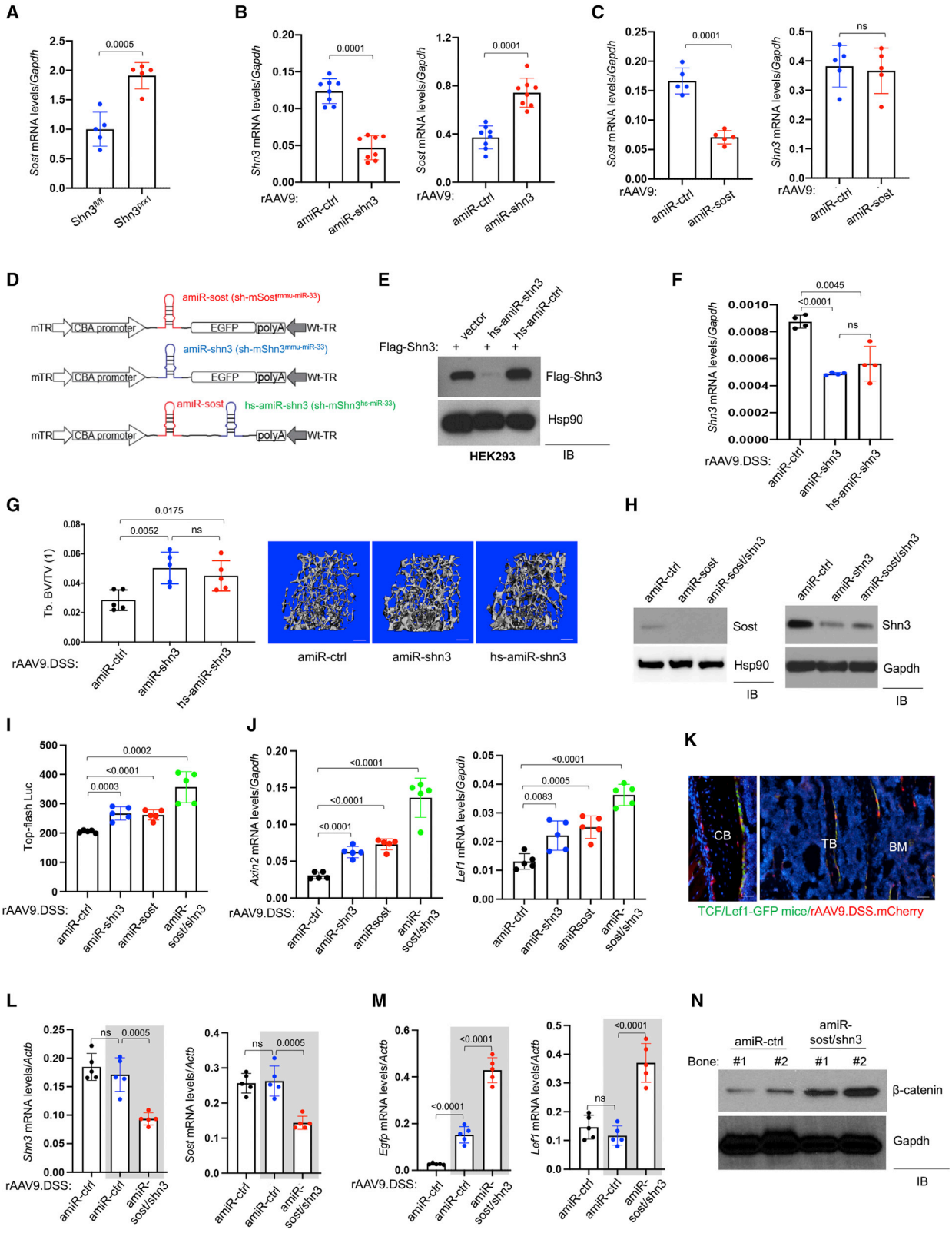

(legend on next page)

shown by lower levels of bone-formation markers 9 months post treatment than at the time of treatment initiation. Additionally, concerns about potential cardiovascular events limit the application of this therapy to a subset of the potentially applicable patients.[12] Based on these limitations, additional anabolic therapeutic targets are needed.

SHN3 is an alternative therapeutic target that can circumvent these limitations. SHN3 is a large, intracellular adaptor protein (>2,000 amino acids) that controls stabilization of β-catenin downstream of WNT signaling (Figure S1).[13] SHN3 acts as a potent inhibitor of bone formation, and its function is intrinsic to osteoblast-lineage cells, as osteoblast-specific deletion of *Shn3* in mice results in a progressive increase in bone mass due to augmented osteoblast activity.[13-16] Moreover, SHN3 inhibition prevented estrogen-deficiency-induced bone loss in mice.[17] Of note, the bone formed in $Shn3^{-/-}$ mice is mature lamellar bone with normal biomechanical properties,[18] and SHN3 deficiency is not associated with phenotypes in non-skeletal tissues.[14] However, despite the therapeutic potentials of SHN3 inhibition in osteoporosis, current therapeutic strategies using antibody-based biologics or small compound molecules are not useful to develop inhibitors targeting the intracellular adaptor protein SHN3 specific to osteoblast-lineage cells.

Recombinant adeno-associated virus (rAAV) has demonstrated high-efficiency transduction of osteoblast-lineage cells in mice,[17] long-term durability of therapeutic gene expression, lack of post-infection immunogenicity, and good safety profiles in clinical studies.[19] Although rAAVs have been evaluated in multiple tissues, such as liver, muscle, heart, eye, and brain, studies of AAV-mediated gene therapy for bone are limited.[20] Using bone-targeted rAAVs carrying artificial microRNA (miRNA) that silence(s) the expression of SHN3, SOST, or a combination of the two, we here find evidence supporting rAAV gene therapy as a complementary approach to traditional osteoporosis drugs. rAAVs are used to deliver long-lasting targeting of WNT signaling components to osteoblast-lineage cells, including the secreted protein SOST and/or the intracellular adaptor protein SHN3. rAAV-mediated silencing of *Shn3* or *Sost* in osteoblast-lineage cells enhanced WNT signaling, osteoblast function, and bone formation in mice. Combination therapy targeting both factors further increased anabolic responses along with reduced bone resorption, compensating for the limitations of single gene silencers, as the expression of SOST and SHN3 is connected via a negative feedback mechanism. Systemic delivery of rAAVs not only counteracted bone loss in both postmenopausal and senile osteoporosis but also promoted the healing of bone fractures or critical-sized bone defects. Furthermore, direct transplantation of an rAAV-bound allograft bone carrying WNT-modulating gene silencers to osteotomy sites markedly improved the healing of critical-sized bone defects. Thus, bone-targeted AAV-mediated regulation of WNT signaling in osteoblast-lineage cells has the potential to treat osteoporosis, bone fractures, and critical-sized bone defects.

RESULTS

Development of WNT-modulating gene silencers using bone-targeted rAAV

The WNT pathway has been considered a promising target for therapeutic intervention in patients with osteoporosis.[21] Our prior work identified SHN3 as a potent osteoblast inhibitor that regulates β-catenin stability via ERK MAPK-mediated suppression of GSK-3β in the context of WNT signaling[14,16] (Figure S1). Intriguingly, among known WNT antagonists,[22] *Sost* expression was highly upregulated in the long bones of *Shn3*-deficient mice (Figure S2B). Likewise, knockdown of *Shn3* expression in the OCY454 osteocyte line upregulated *Sost* expression, while *Dkk1* expression was unchanged in *Shn3*-deficient osteoblasts (Figures S2C and S2D), suggesting that SHN3 controls *Sost* expression in osteocytes. Accordingly, osteoblast-specific deletion of *Shn3* ($shn3^{prx1}$; Figure 1A) or intravenous (i.v.) injection with an rAAV9 carrying an artificial miRNA (amiR) that silences *Shn3* expression in osteoblast-lineage cells (rAAV9.

Figure 1. Generation of bone-targeted AAV carrying WNT-modulating gene silencers

(A) mRNA levels of *Sost* in the tibias of 3-month-old wild-type (WT) ($Shn3^{fl/fl}$) and $Shn3^{prx1}$ mice (n = 5). (B and C) mRNA levels of *Shn3* and *Sost* in the tibias of 3-month-old WT mice treated with rAAV9 carrying *amiR-ctrl*, *amiR-shn3* (B, n = 8), or *amiR-sost* (C, n = 5). (D) Diagram of the AAV vector genome containing a cytomegalovirus (CMV) enhancer/chicken β-actin promoter (CBA), *amiR-sost (sh-mSost*$^{mmu\text{-}miR\text{-}33}$*)*, *amiR-shn3 (sh-mShn3*$^{mmu\text{-}miR\text{-}33}$*)*, or *amiR-sost/hs-amiR-shn3 (sh-mSost*$^{mmu\text{-}miR\text{-}33}$*;sh-mShn3*$^{hs\text{-}miR\text{-}33}$*)*, an *Egfp* reporter gene (EGFP), *β-globin* polyA sequence (polyA), and mutant (m) or WT terminal repeat (TR). (E) A FLAG-Shn3-expressing plasmid was transfected into HEK293 cells along with vector control or a plasmid encoding *hs-amiR-shn3* or *amiR-ctrl*, and, 2 days later, cell lysates were immunoblotted for FLAG-Shn3 or Hsp90 (as a loading control). (F and G) rAAV9.DSS (5×10^{13} vg/kg) carrying *amiR-ctrl*, *amiR-shn3*, or *hs-amiR-shn3* was injected i.v. into 2-month-old mice, and, 2 months later, mRNA levels of *Shn3* in the tibias were measured by RT-PCR and normalized to *Gapdh* (F). MicroCT analysis showing trabecular bone mass in AAV-treated femurs. Relative quantification (G, left) and representative 3D-reconstructions (G, right) are displayed. Tb.BV/TV, trabecular bone volume/total volume. Scale bar, 500 μm. (H–J) Ocy454 osteocytic cells were incubated with rAAV9.DSS carrying *amiR-ctrl*, *amiR-shn3*, *amiR-sost*, or *amiR-shn3/sost* for 2 days, cultured under differentiation conditions for 6 days, and immunoblotted with the indicated antibodies (H). AAV-treated Ocy454 cells were transfected with a β-catenin-responsive reporter gene (Top-flash Luc), cultured for 6 days in the presence of rWNT3a, and luciferase activity was measured (I, n = 4). Alternatively, mRNA levels of β-catenin target genes, *Axin2* and *Lef1*, were assessed by RT-PCR and normalized to *Gapdh* (J, n = 5). (K–N) Two-month-old TCF/LEF1-GFP reporter mice were i.v. injected with rAAV9.DSS.*mCherry* (5×10^{13} vg/kg), and, 2 weeks later, expression of GFP and mCherry in the femurs was visualized by fluorescence microscopy (K, n = 3). Scale bar, 100 μm. CB, cortical bone; TB, trabecular bone; BM, bone marrow. Alternatively, rAAV9.DSS (5×10^{13} vg/kg) carrying *amiR-ctrl* or *amiR-sost/shn3* were i.v. injected into WT or TCF/LEF1-GFP reporter (gray box) mice, and, 2 weeks later, mRNA levels of *Shn3* and *Sost* (L) and *egfp* and *Lef1* (M) in the tibia were measured by RT-PCR and normalized to *Actb* (n = 5). Protein lysates from the femur were immunoblotted for β-catenin. Gapdh was used as a loading control (N). WT mice were used as a negative control. Values represent mean ± SD by an unpaired two-tailed Student's t test (A–C) and one-way ANOVA test (F, G, I, J, L, and M). ns, not significant.

amiR-shn3)[17] (Figure 1B) also upregulated *Sost* expression, suggesting that SHN3 deficiency in osteoblast-lineage cells results in an increase in *Sost* expression. However, rAAV9-mediated silencing of *Sost* expression (rAAV9.*amiR-sost3*) did not affect *Shn3* expression in the tibia (Figure 1C). This observation suggests that *Shn3* deficiency in osteoblast-lineage cells may induce a negative feedback pathway that blunts WNT/β-catenin activation via upregulation of *Sost*, but not other WNT antagonists, including *Sfrp1*, *Sfrp2*, and *Dkk1*. However, this regulation was not bidirectional as there is no effect of *Sost* deficiency on SHN3 expression. Further study will be necessary to define how SHN3 controls *Sost* expression in osteocytes.

To test whether expression of SHN3 and SOST is connected via a negative feedback mechanism, we hypothesized that inhibition of both factors could further increase WNT/β-catenin signaling in osteoblast-lineage cells. A bone-targeted AAV9 capsid was rationally designed by grafting a bone-homing $(AspSerSer)_6$ peptide motif onto an AAV9-VP2 capsid protein (AAV9.DSS) to detarget non-skeletal tissues, including liver, heart, and muscle.[17,23] Additionally, given that high levels of AAV-delivered short hairpin RNAs (shRNAs) may induce cytotoxicity by perturbing RNA interference machinery or exhibit significant off-target silencing,[24,25] an AAV-compatible amiR was developed by embedding the guide strand of a small silencing RNA that targets *Sost* or *Shn3* into a mouse miR-33-derived miRNA scaffold (*amiR-sost*, *amiR-shn3*). This strategy enables efficient gene knockdown, increases vector genome integrity, and limits shRNA-related toxicity, while reducing off-target silencing 10-fold compared with conventional shRNA constructs.[26] Finally, we developed rAAV that targets both *Sost* and *Shn3* in osteoblast-lineage cells for a combination therapy. To maximize co-expression of *amiR-sost* and *amiR-shn3* in the same cells, two amiRs were inserted into a single AAV vector genome. To avoid potential incomplete transcription of the juxtaposed amiRs by redundant nucleotide sequences,[27] the target sequences for *Shn3* were embedded into a human miR-33-derived miRNA scaffold (hs-amiR) (Figures 1D and S3A). Immunoblotting analysis validated its knockdown efficiency in HEK293 cells (Figure 1E). Two-month-old wild-type (WT), injected i.v. with rAAV9.DSS carrying *amiR-shn3* or *hs-amiR-shn3*, showed a ∼40% reduction in *Shn3* mRNA levels in the tibia (Figure 1F) and a corresponding increase in femoral bone mass (Figure 1G). These results demonstrate that *hs-amiR-shn3* is as effective as *amiR-shn3* in silencing *Shn3* expression in the tibia and increasing bone accrual. For a combinatory therapy, *hs-amiR-shn3* was inserted between *amiR-sost* and poly-adenylation (poly(A)) sites and packaging into the rAAV9.DSS capsid (AAV9.DSS.*amiR-sost/shn3*; Figure 1D).

Bone-targeted AAV gene silencers are fine-modulators of WNT signaling in the skeleton

To compare the ability of a gene silencer targeting *Sost* or *Shn3* alone, or *Shn3* and *Sost* together, to enhance WNT/β-catenin signaling *in vitro*, SOST-expressing Ocy454 osteocytic cells[28] were transduced with an rAAV9.DSS carrying *amiR-shn3*, *amiR-sost*, or *amiR-sost/shn3*, and knockdown efficiency in these cells was validated by immunoblotting (Figure 1H) and RT-PCR analyses (Figure S3B). Treatment with *amiR-shn3* or *amiR-sost* resulted in a mild increase in β-catenin transcriptional activity (Top-flash Luc) in Ocy454 cells while β-catenin activity was further increased when *Shn3* and *Sost* were both silenced (Figure 1I). This effect corresponded to upregulated expression of the β-catenin target genes, *Axin2* and *Lef1* (Figure 1J). These results demonstrated that bone-targeted AAV9-mediated silencing of *Shn3*, *Sost*, or *Shn3/Sost* in combination acts as a robust modulator of WNT/β-catenin signaling in osteoblast-lineage cells.

In vivo transduction of WNT-responsive osteoblast-lineage cells with a systemically delivered rAAV9.DSS was examined using transgenic TCF/Lef1-GFP reporter mice that express a fused protein of histone 2B and GFP in response to WNT stimulation.[29] These mice were injected i.v. with an mCherry-expressing rAAV9.DSS, and, 2 weeks later, GFP and/or mCherry expression in the femur was visualized by fluorescence microscopy (Figure 1K). Co-labeling with these two reporters confirmed that systemic delivery of rAAV9.DSS efficiently transduced a subset of WNT-responsive osteoblasts and osteocytes. Next, rAAV9.DSS.*amiR-sost/shn3* was injected i.v. into TCF/Lef1-GFP mice to test the ability of dual silencing of *Shn3* and *Sost* to increase WNT signaling *in vivo*. Efficient knockdown of *Shn3* and *Sost* expression in the tibia was confirmed 2 weeks post injection (Figure 1L). As seen in *Shn3*/*Sost*-deficient Ocy454 cells, silencing of *Shn3* and *Sost* markedly increased WNT/β-catenin signaling in long bones, indicated by greater expression of the WNT-responsive GFP, WNT-target gene (*Lef1*; Figure 1M) and β-catenin protein levels (Figure 1N). Thus, dual silencing of *Shn3* and *Sost* via a bone-targeted rAAV effectively enhanced WNT/β-catenin signaling in the skeleton.

Bone-targeted AAV gene silencers increase bone accrual in mice

Canonical WNT signaling in osteoblasts has been reported to inhibit osteoclastogenesis by increasing osteoprotegerin (OPG, *Tnfrsf11b*) production.[30] Similarly, *amiR-sost/shn3* treatment significantly upregulated *Opg* transcripts in the tibia 2 weeks post injection but did not affect the expression of receptor activator of nuclear factor κB (NF-κB) ligand (RANKL, *Tnfsf11*; Figure 2A), demonstrating that hyperactivation of WNT/β-catenin signaling by deficiency of *Shn3* and *Sost* upregulates *Opg* expression *in vivo*. Remarkably, this effect was accompanied by a significant increase in trabecular bone mass in the metaphyseal areas of long bones and vertebrae with high bone remodeling activity, resembling the skeletal phenotypes of mice treated with an OPG inhibitor, OPG-Fc fragment (Figures 2B and S4). Of note, *amiR-sost/shn3* treatment rapidly induced a substantial anabolic response along with reduced osteoclast numbers, increasing trabecular bone mass by ∼2.5-fold in the femur within 2 weeks (Figures 2C and 2J).

To examine *in vivo* correspondence of AAV-mediated silencing of *Shn3*, *Sost*, or *Shn3/Sost* in combination with WNT/β-catenin signaling and bone accrual, rAAV9.DSS carrying *amiR-ctrl*, *amiR-shn3*, *amiR-sost*, or *amiR-sost/shn3* were injected i.v. into 2-month-old WT mice. Four weeks later, the knockdown efficiency of *Shn3*

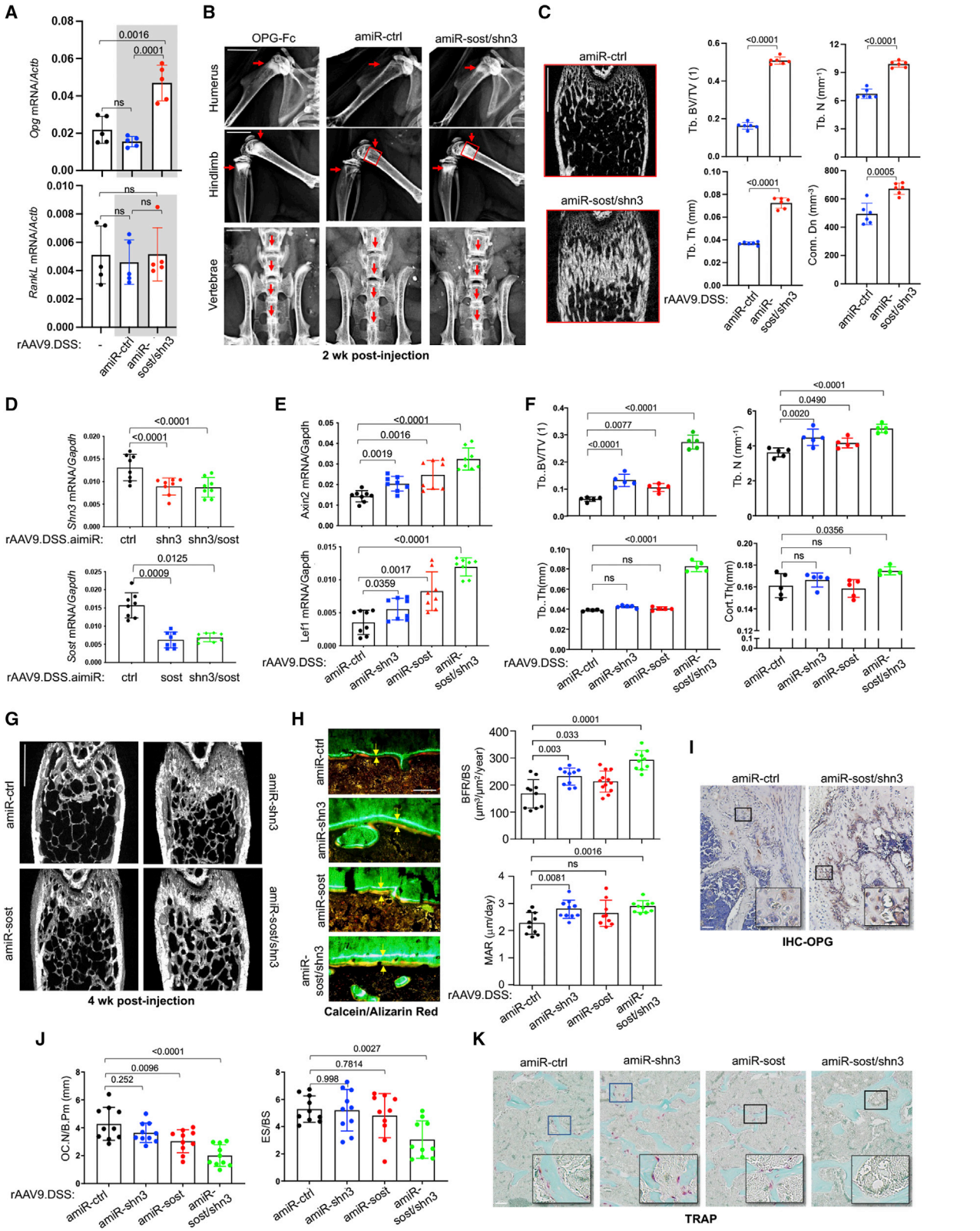

(legend on next page)

or *Sost* in the tibia was examined, demonstrating that amiRs targeting *Shn3*, *Sost*, or the combination had an equivalent reduction in *Shn3* or *Sost* mRNA levels (Figure 2D). Compared with a mild induction in WNT-responsive genes in tibias treated with *amiR-shn3* or *amiR-sost*, gene induction was markedly increased in the presence of *amiR-sost/shn3* (Figure 2E). This increase corresponded to an increase in trabecular bone mass and cortical bone thickness in AAV-treated femurs (Figures 2F and 2G). Similarly, *in vivo* osteoblast activity was markedly increased in *amiR-sost/shn3*-treated femurs compared with femurs treated with *amiR-shn3* or *amiR-sost* that only showed a mild increase in bone-formation rate (BFR) and mineral apposition rate (MAR) (Figure 2H). Additionally, *amiR-sost/shn3* treatment enhanced WNT/β-catenin signaling in the femur (Figure 2E); accordingly, *Opg* expression in osteoblasts and osteocytes was highly upregulated (Figure 2I). This result was accompanied by a significant decrease in the numbers of tartrate-resistant acid phosphatase (TRAP)-positive osteoclasts per bone surface (Figure 2J) and bone erosion area per bone surface (Figure 2K). However, TRAP-positive osteoclast numbers and bone resorption activity were unchanged in femurs treated with *amiR-shn3* or *amiR-sost*, demonstrating that, unlike the dual silencer, the single silencers did not affect osteoclast differentiation and resorption activity (Figures 2J and 2K). Notably, the *in vitro* osteoclast differentiation and resorption activity were largely normal in bone marrow-derived monocytes (BMMs) treated with *amiR-shn3*, *amiR-sost*, or *amiR-sost/shn3* (Figure S5), demonstrating no intrinsic effect of WNT-modulating gene silencers on osteoclast differentiation and function. Taken together, systemic delivery of rAAV9.DSS.*amiR-sost/shn3* to osteoblast-lineage cells enhances WNT/β-catenin signaling, which not only promoted osteoblast-mediated bone formation but also suppressed osteoclast-mediated bone resorption via *Opg* upregulation. On the other hand, treatment with *amiR-shn3* or *amiR-sost* resulted in a mild increase in WNT/β-catenin signaling, promoting osteoblast-mediated bone formation without any detectable alteration in osteoclast development.

Bone-targeted AAV gene silencers reverse bone loss in osteoporotic mice

Postmenopausal and aging-associated osteoporosis result in bone loss and deterioration of bone structure, increasing the risk of fracture.[31] Our data showing elevated *Shn3* and *Sost* mRNA levels in osteoporotic bones (Figure 3A) prompted us to examine the therapeutic effects of silencing of *Shn3*, *Sost*, or *Shn3*/*Sost* in combination in mouse models of osteoporosis. Ovariectomized (OVX) mice[32] were utilized as a model for postmenopausal osteoporosis. Sham control or OVX surgery was conducted in 12-week-old female mice and, 6 weeks later, a single dose of rAAV9.DSS carrying *amiR-ctrl*, *amiR-shn3*, *amiR-sost*, or *amiR-sost/shn3* was injected i.v. (Figure 3B). Eight weeks after injection, reduced levels of *Shn3* and/or *Sost* mRNAs were seen in AAV-treated OVX tibias (Figure 3C). While *amiR-ctrl*-treated OVX mice showed a significant reduction in trabecular bone mass compared with sham mice, this bone loss was partially or almost completely reversed by treatment with *amiR-sost* or *amiR-shn3*, respectively, as shown by greater trabecular BV/TV, thickness, and connectivity density (Figures 3D and 3E). Intriguingly, *amiR-shn3* treatment was more effective in increasing trabecular than cortical bone mass (Figure 3E), while *amiR-sost* treatment was more effective in increasing cortical than trabecular bone mass (Figure S6A). These results suggest that AAV-mediated silencing of *Shn3* shows functional selectivity for osteoblast function in the trabecular bone within the metaphyseal region with high bone remodeling activity. In contrast, AAV-mediated silencing of *Sost* in osteocytes primarily affects the osteoblasts residing on the surface of cortical bone in close proximity to osteocytes. Remarkably, *amiR-sost/shn3* treatment caused a substantial increase in trabecular bone mass, resulting in a ~2-fold increase in trabecular BV/TV versus that of sham mice or mice treated with *amiR-shn3* or *amiR-sost*. These results suggest that single silencing of *Shn3* reversed estrogen-deficiency-induced bone loss more effectively than single silencing of *Sost* and was further improved when *Shn3* and *Sost* were both silenced.

To examine the therapeutic effects of AAVs on aging-associated osteoporosis, we injected 20-month-old male mice i.v. with a single dose of rAAV9.DSS carrying *amiR-ctrl*, *amiR-shn3*, *amiR-sost*, or *amiR-sost/shn3*. Two months later, AAV-treated tibias had reduced *Shn3* and *Sost* mRNA levels Figure 3F). Compared with *amiR-ctrl*-treated mice, *amiR-sost/shn3*-treated mice showed a significant increase in trabecular bone mass, while treatment with *amiR-shn3* or *amiR-sost* resulted in a mild increase (Figures 3G and 3H). Lumbar vertebrae (L4) from AAV-treated mice also showed similar increases in trabecular bone mass (Figures 3I and S6B). These results demonstrated that bone-targeted rAAV9-mediated delivery of WNT-modulating

Figure 2. Bone-targeted AAV gene silencers increase bone formation in mice

(A–C) Two-month-old WT and TCF/Lef1-GFP reporter (gray box) mice were injected i.v. with rAAV9.DSS (5×10^{13} vg/kg) carrying *amiR-ctrl* or *amiR-sost/shn3*, and, 2 weeks later, mRNA levels of *Opg* and *RankL* in the tibia were measured by RT-PCR and normalized to *Actb* (A, n = 5). Bone accrual in the metaphyseal areas of humerus, hindlimb, and vertebrae was assessed by radiography (red arrows). Alternatively, OPG-Fc (1 mg/kg) was intraperitoneally (i.p.) injected weekly into 2-month-old WT mice (B, n = 3). Femoral bone mass was assessed by microCT. Red box in (B) shows representative 2D-transsection (C, left) and relative quantification (C, right) are displayed (n = 6). Tb.BV/TV, trabecular bone volume/total volume; Tb.N, trabecular number; Tb.Th, trabecular thickness; Condon, connective density. Scale bars, (B) 50 μm, (C) 1 mm. (D–K) Two-month-old WT mice were i.v. injected with rAAV9.DSS (5×10^{13} vg/kg) carrying *amiR-ctrl*, *amiR-shn3*, *amiR-sost*, or *amiR-sost/shn3*, and, 4 weeks later, mRNA levels of *Shn3* and *Sost* (D) and *Axin2* and *Lef1* (E) in the tibia were measured by RT-PCR and normalized to *Gapdh* (n = 8). Femoral bone mass was assessed by microCT (F, G). Representative 3D-reconstruction (G) and relative quantification (F) are displayed (n = 8). Cort.Th, cortical thickness. Scale bar, 1 mm. Dynamic histomorphometry was performed in the metaphysis of AAV-treated femurs (H and J). (H) (Left) Representative calcein/alizarin red labeling (arrows indicate the distance between calcein and alizarin red labeling); (right) relative histomorphometric quantification of bone-formation rate (BFR)/bone surface (BS) and mineral apposition rate (MAR). (I) IHC for OPG was performed in AAV-treated femurs. (J and K) Plots showing quantification of OC.N/B.Pm and ES/BS (J) and representative images from TRAP staining (K) (n = 10). Scale bars: (G) 1 mm, (H) 50 μm, (I) 100 μm, (K) 100 μm. Values represent mean ± SD by an unpaired two-tailed Student's t test (C) and one-way ANOVA test (A, D–F, H, J).

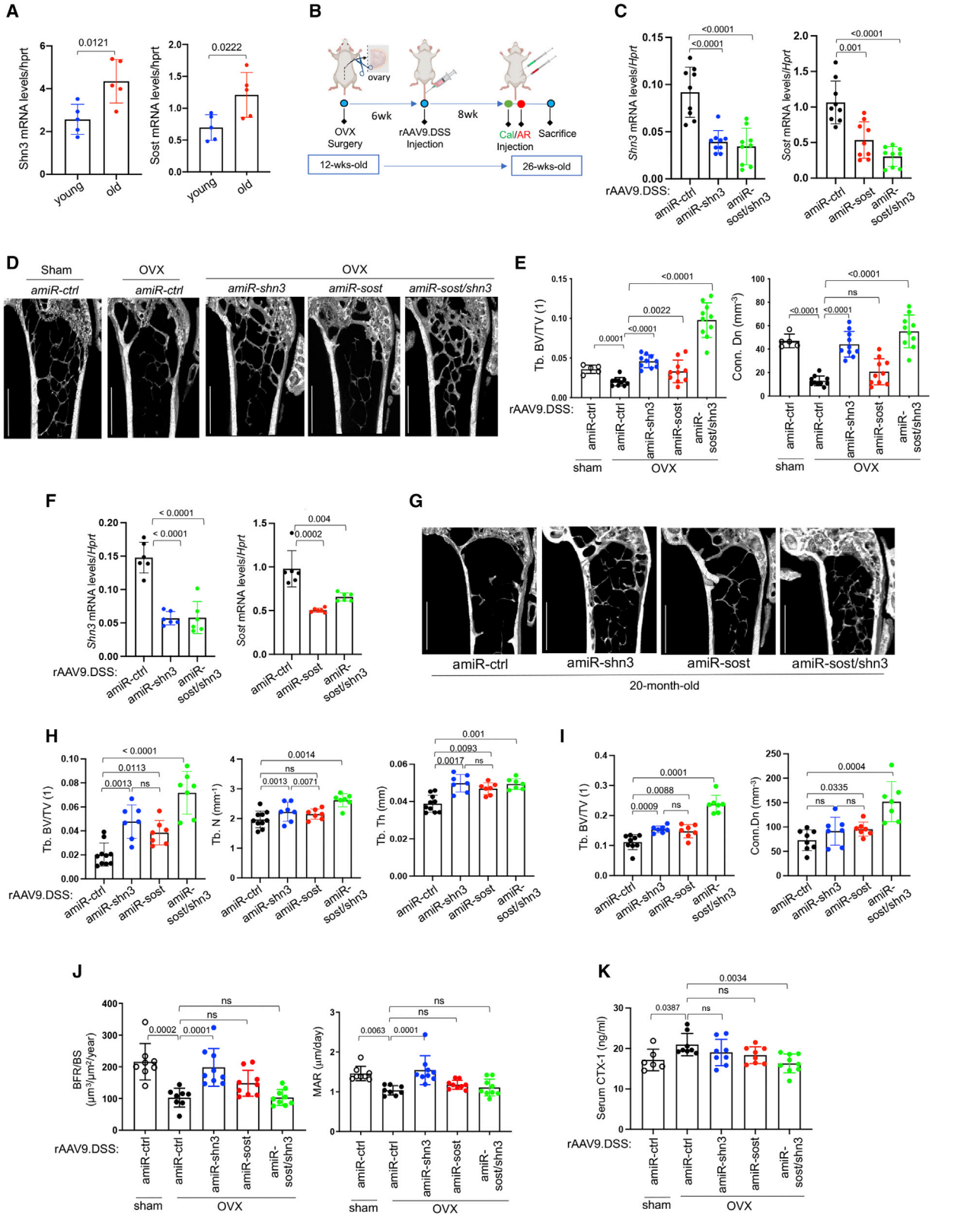

(legend on next page)

silencers effectively counteracted bone loss in both aging-associated and postmenopausal osteoporosis.

While *amiR-sost/shn3* treatment led to a significant increase in bone mass 8 weeks post injection, it did not affect *in vivo* osteoblast activity (Figure 3J) but induced a significant decrease in *in vivo* osteoclast activity (Figure 3K). Unlike *amiR-sost/shn3*, *amiR-shn3*-treated femurs showed a sustained increase in osteoblast activity without any alteration in osteoclast activity, whereas only a mild change in osteoblast and osteoclast activity was observed in *amiR-sost*-treated femurs (Figures 3J and 3K). Upon treatment with *amiR-sost/shn3*, osteoblast-mediated bone formation wanes over time along with a decrease in osteoclast-mediated bone resorption. Unlike *amiR-sost/shn3*, *amiR-shn3* treatment almost completely reversed osteoporosis by promoting osteoblast-mediated bone formation without any alteration in osteoclast function. In contrast, bone loss was only partially reversed by *amiR-sost* treatment, which induced a mild increase in osteoblast function and a mild decrease in osteoclast function. Taken together, systemic delivery of bone-targeted rAAV carrying gene silencers targeting *Shn3*, *Sost*, or both could be a promising therapeutic approach for both postmenopausal and aging-associated osteoporosis.

Bone-targeted AAV gene silencers promote bone regeneration

A 3-mm length of cortical bone defect in the femur is an established surgical model to test bone regeneration activity while limiting mechanical instability at the bone-injury site by preserving other cortical bone at the level of the bone defect (Figure S7A).[33,34] Eight-week-old mice were injected i.v. with GFP-expressing rAAV9.DSS 2 weeks prior to surgery and, 2 weeks after surgery, GFP expression was monitored by fluorescence microscopy of the injury site (Figure S7B). This analysis demonstrated that systemically delivered rAAV9.DSS efficiently transduced skeletal cells at the bone defect site (Figures 4A and S7C). Next, bone formation at the defect sites was assessed by micro-computed tomography (microCT) and histology 2 weeks after i.v. injection of rAAV9.DSS carrying *amiR-shn3*, *amiR-sost*, or *amiR-sost/shn3*. All three AAV vectors increased bone formation, collagen production (Figures 4B and 4C), and osteoblast numbers (Figure 4D, left) in the bone defect sites, demonstrating the bone regeneration activity of WNT-modulating gene silencers in a cortical defect model. Of note, *amiR-sost/shn3* treatment reduced osteoclast numbers in the cortical defect areas, while osteoclast numbers were relatively normal in the presence of *amiR-shn3* or *amiR-sost* (Figure 4D, right). Thus, single and dual silencing of *Shn3* and *Sost* were both effective in promoting bone formation during the early stages of bone defect healing; however, only the dual silencer showed an antiresorptive effect.

Therapeutic effects of bone-targeted AAV gene silencers on bone fracture healing

Our data showing elevated expression of *Shn3* and *Sost* during bone regeneration after cortical injury suggests that SHN3 and/or SOST may function as a negative regulator of bone fracture healing (Figure S8A). To test the ability of silencing of *Shn3*, *Sost*, or both to promote bone fracture healing, a surgical fracture was created in the left femur 2 weeks after i.v. injection of an rAAV9.DSS carrying *egfp*, *amiR-ctrl*, *amiR-shn3*, *amiR-sost*, or *amiR-sost/shn3*. The femur was stabilized with an intramedullary rod following femoral osteotomy (Figure S8B). Fluorescence microscopy analysis of *egfp*-treated mice demonstrated that GFP-expressing cells were present in the fracture callus 1 week post surgery, and their abundance increased at 2 weeks and gradually decreased at 4 weeks (Figures 4E and S8C). A subset of GFP-expressing cells were osteocalcin (*Bglap*)-positive mature osteoblasts and/or SOST-positive osteocytes (Figure S8D). This result suggests that osteoblast-lineage cells undergoing initial dynamic proliferation in response to injury are effectively transduced by a systemically delivered rAAV9.DSS. Notably, GFP expression in AAV-transduced cells decreases at 4 weeks as AAVs' genome copy numbers are reduced during cell proliferation.[19] Next, reduced expression of *Shn3* and/or *Sost* was validated in the tibias treated with *amiR-shn3*, *amiR-sost*, or *amiR-sost/shn3* (Figure 4F). As expected, treatment with *amiR-shn3* or *amiR-sost* led to a mild increase in WNT-responsive gene expression (*Axin2*, *Lef1*) and trabecular bone mass in contralateral bones without the surgery, both of which were further increased by treatment with the combined *amiR-sost/shn3* (Figures 4G, 4H, S9A, and S9B). These results confirmed the effectiveness of systemically delivered AAV vectors to increase WNT/β-catenin signaling and bone accrual in mice. Notably, expression of *Axin2* and *Lef1* in the skeletal muscle adjacent to fractured femurs was unchanged by the treatment with *amiR-shn3/sost*, suggesting that the effect of AAV-mediated silencing of *Shn3* and/or *Sost* to regulate WNT/β-catenin signaling is specific to the bone (Figure S9C).

Only ∼40% of *amiR-ctrl*-treated femurs showed fracture union 6 weeks after the surgery, and this union rate was markedly improved by ∼87% or ∼93% when treated with *amiR-shn3* or *amiR-sost*, respectively. Despite a significant increase in callus formation in the

Figure 3. Bone-targeted AAV gene silencers reverse bone loss in osteoporosis

(A) mRNA levels of *Shn3* or *Sost* in the tibia of young (2-month-old) or old (20-month-old) mice (n = 5). (B) Diagram of the study and treatment methods. (C–E) Sham or OVX surgery was performed on 3-month-old female mice, and, 6 weeks later, mice were i.v. injected with rAAV9.DSS (5×10^{13} vg/kg) carrying *amiR-ctrl*, *amiR-shn3*, *amiR-sost*, or *amiR-sost/shn3*. Eight weeks later, mRNA levels of *Shn3* and *Sost* in the tibia were assessed by RT-PCR and normalized to *Hprt* (C, n = 9). Femoral bone mass was assessed by microCT (D and E). Representative 3D-reconstruction (D) and relative quantification (E) are displayed (n = 5–10). Scale bar: (D) 1 mm. (F–I) Twenty-month-old male mice were i.v. injected with rAAV9.DSS (5×10^{13} vg/kg) carrying *amiR-ctrl*, *amiR-shn3*, *amiR-sost*, *or amiR-sost/shn3*, and, 2 months later, mRNA levels of *Shn3* and *Sost* in the tibia were assessed by RT-PCR and normalized to *Hprt* (F, n = 6). Trabecular bone mass in femurs (G and H) and lumbar vertebrae (L4, I) were assessed by microCT. Representative 3D reconstruction (G) and relative quantification (H and I) are displayed (n = 8–10). Scale bar: (G) 1 mm. (J and K) Sham or OVX surgery was performed on 3-month-old female mice, and, 6 weeks later, mice were i.v. injected with rAAV9.DSS. Histomorphometric quantification of BFR/BS and MAR was performed 8 weeks post injection (J). Serum CTX-I levels were measured to assess *in vivo* osteoclast activity (K). Values represent mean ± SD by an unpaired two-tailed Student's t test (A) and one-way ANOVA test (C, E, F, H–K).

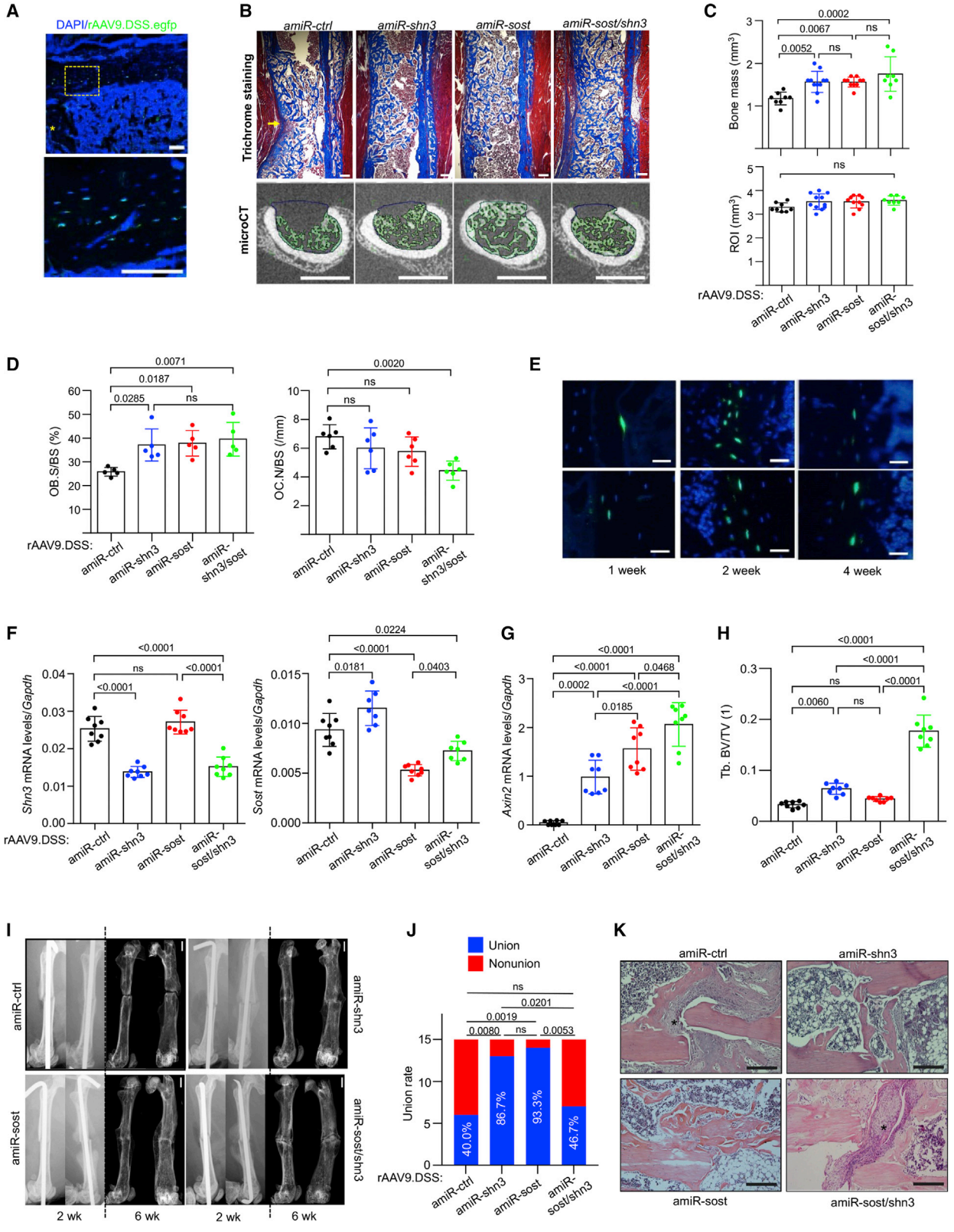

(legend on next page)

fractured sites (Figure S9D), little to mild increase in union rate was detected in *amiR-sost/shn3*-treated femurs (Figures 4I and 4J). This is consistent with histologic analyses showing that treatment with *amiR-shn3* or *amiR-sost* markedly enhanced connectivity between fracture ends due to augmented bone formation, whereas *amiR-ctrl*- or *amiR-sost/shn3*-treated femurs developed fibrotic tissue in the non-union sites (Figure 4K). Intriguingly, these non-union sites in *amiR-sost/shn3*-treated femurs showed a significant decrease in numbers of TRAP-positive osteoclasts, while osteoclast numbers at fracture sites were comparable between the femurs treated with *amiR-ctrl*, *amiR-shn3*, or *amiR-sost* (Figures S9E and S9F). A previous study reported that constitutive activation of β-catenin significantly increased bone mass but decreased the bone remodeling process, resulting in delayed bone fracture healing in mice.[35] Thus, hyperactivation of WNT/β-catenin signaling in *amiR-sost/shn3*-treated femurs may also slow down bone remodeling during fracture repair due to reduced osteoclast development, resulting in delayed fracture union, although its bone regeneration activity during the early healing process is enhanced. On the other hand, a mild increase in WNT/β-catenin signaling by single silencing of *Shn3* or *Sost* promoted osteoblast-mediated bone formation without disturbing osteoclast development and bone remodeling, which enhanced fracture repair (Table S1).

Development of a bone-anabolic, human skeletal organoid

The healing of critical-sized bone defects remains one of the most challenging problems in orthopedic management, which requires the implantation of a bone graft equipped with optimal osteoconductive, osteoinductive, and osteogenic activities.[36] To develop a skeletal organoid with a high bone-forming activity, mouse or human bone marrow-derived mesenchymal stromal cells (BMSCs) were seeded on an allograft or synthetic bone expressing *amiR-shn3*. An AAV9 capsid with the bone-targeting peptide motifs, $(Asp\text{-}Ser\text{-}Ser)_6$[37] or $(Asp)_{14}$[38] (rAAV9.DSS, rAAV9.D14) was engineered to bind an allograft bone or hydroxyapatite (HA)-based scaffold[39] (Figure S10A). After incubation with decellularized allograft bone or an HA scaffold, its binding affinity was assessed by measuring the bone/scaffold-bound AAV genome copies (GCs; Figure 5A). While WT rAAV9 (rAAV9.WT) showed little to no binding affinity to allograft bone or the HA scaffold, its binding affinity was markedly improved when grafted with DSS or D14 peptide motifs. Notably, the rAAV9.DSS capsid has a higher binding affinity to both allograft bone and the HA scaffold than that of rAAV9.D14, as shown by greater numbers of AAV GCs (Figure 5A). Since HA is a major inorganic component of bone, HA is likely to mediate the interaction between the rAAV9.DSS capsid and allograft bones. Consistent with this, rAAV9.DSS.*egfp* effectively transduced fresh human bone tissue in the culture (Figure 5B) as well as mouse and human BMSCs (Figure 5C), as shown by GFP expression. Since the rAAV9.DSS capsid directly binds to the HA scaffold, rAAV9.DSS.*egfp* was incubated with the HA scaffold for 1 h, then mouse or human BMSCs were seeded onto the AAV-bound scaffold (Figure 5D). Both mouse and human BMSCs on the surface of the AAV-bound scaffold highly expressed GFP (Figures 5E and 5F), suggesting that rAAV9.DSS attaching to the HA scaffold effectively transduces mouse or human osteoblast-lineage cells to ultimately generate skeletal organoids.

As SHN3 functions as an endogenous inhibitor of osteoblast function in mice,[13,40] overexpression of SHN3 inhibited osteogenic differentiation of human BMSCs (Figure S10B), whereas osteoblast differentiation was enhanced by shRNA-mediated knockdown of *SHN3* (Figure S10C). The same nucleotide sequences targeting human *SHN3* mRNA were embedded into human miR-33-derived miRNA scaffold-based cassettes (*hs-amR-hSHN3*) and then packaged into rAAV9.DSS capsid (Figure 5G). The AAV's ability to transduce human BMSCs was assessed by GFP expression using fluorescence microscopy (Figure 5H), and its knockdown efficiency and osteogenic effects were examined by RT-PCR (Figure 5I). To develop a bone-anabolic, human skeletal organoid, human BMSCs were seeded onto the rAAV9.DSS.*hs-amiR-hSHN3*-bound HA scaffold and then incubated under osteogenic culture conditions for 2 days. This organoid was implanted into interscapular fat pads of immunodeficient mice, and, 4 weeks later, bone formation was assessed by radiography, microCT, and histology (Figures S10D and S10E). Bone accrual (microCT), osteoblast numbers (immunohistochemistry [IHC]-BGLAP), and collagen production (trichrome) were all markedly increased in HA-scaffolds treated with *hs-amiR-hSHN3* relative to those treated with *hs-amiR-ctrl* (Figures 5J and 5K). Taken together, the rAAV9.DSS-bound HA scaffold is effective for the delivery of

Figure 4. Bone-targeted AAV gene silencers promote bone regeneration in mice

(A) rAAV9.DSS.egfp (5×10^{13} vg/kg) was injected i.v. into 2-month-old mice, and, 2 weeks later, a 3-mm length of cortical bone defect was generated on the lateral aspect of the left femur. GFP expression in the cryo-sectioned femurs was monitored by fluorescence microscopy 2 weeks post surgery (n = 3). Scale bar: 100 μm. (B–D) Two-month-old mice were i.v. injected with rAAV9.DSS (5×10^{13} vg/kg) carrying *amiR-ctrl*, *amiR-shn3*, *amiR-sost*, or *amiR-sost/shn3*, and, 2 weeks later, cortical bone defect surgery was performed on the lateral aspect of the left femur. Newly formed bones in the defect areas were assessed by microCT and histology 2 weeks after the surgery (B and C). Representative trichrome-stained longitudinal sections of femurs (B, top), 2D cross-sectional microCT images (B, bottom), and relative quantification of bone volume, region of interest (ROI, C), Ob.S/BS (and osteoclast numbers per bone surface (Oc.N/BS) (D) are displayed (n = 8). Scale bars: (B, top) 200 μm, (B, bottom) 1 mm. (E) Three-month-old mice were i.v. injected with rAAV9.DSS.*egfp* (5×10^{13} vg/kg), and, 2 weeks later, femoral osteotomy and intramedullary fixation were performed. GFP expression on the cryo-sectioned femurs was assessed by fluorescence microscopy 1, 2, and 4 weeks postoperatively. Scale bars: (B) 200 μm, (E) 25 μm. (F–K) Three-month-old mice were i.v. injected with rAAV9.DSS (5×10^{13} vg/kg) carrying *amiR-ctrl*, *amiR-shn3*, *amiR-sost*, or *amiR-sost/shn3*, and, 2 weeks later, femoral osteotomy and intramedullary fixation were performed. Six weeks after the surgery, mRNA levels of *Shn3* and *Sost* (F) and *Axin2* (G) in the tibia were assessed by RT-PCR and normalized to *Gapdh* (n = 8). Tb.BV/TV in the contralateral femurs was assessed by microCT (H, n = 8). Representative radiography and microCT images of the fractured femurs 2 and 6 weeks post surgery are displayed, respectively (I). Union rate at the fracture sites was quantitated by microCT (J). Representative H&E-stained longitudinal sections of femurs at the fracture sites 6 weeks post surgery are displayed (K). Asterisk (*) indicates fibrous tissues at persistent non-union sites. Scale bars: (I) 1 mm, (K) 200 μm. Values represent mean ± SD by a one-way ANOVA test (C, D, F–H, J).

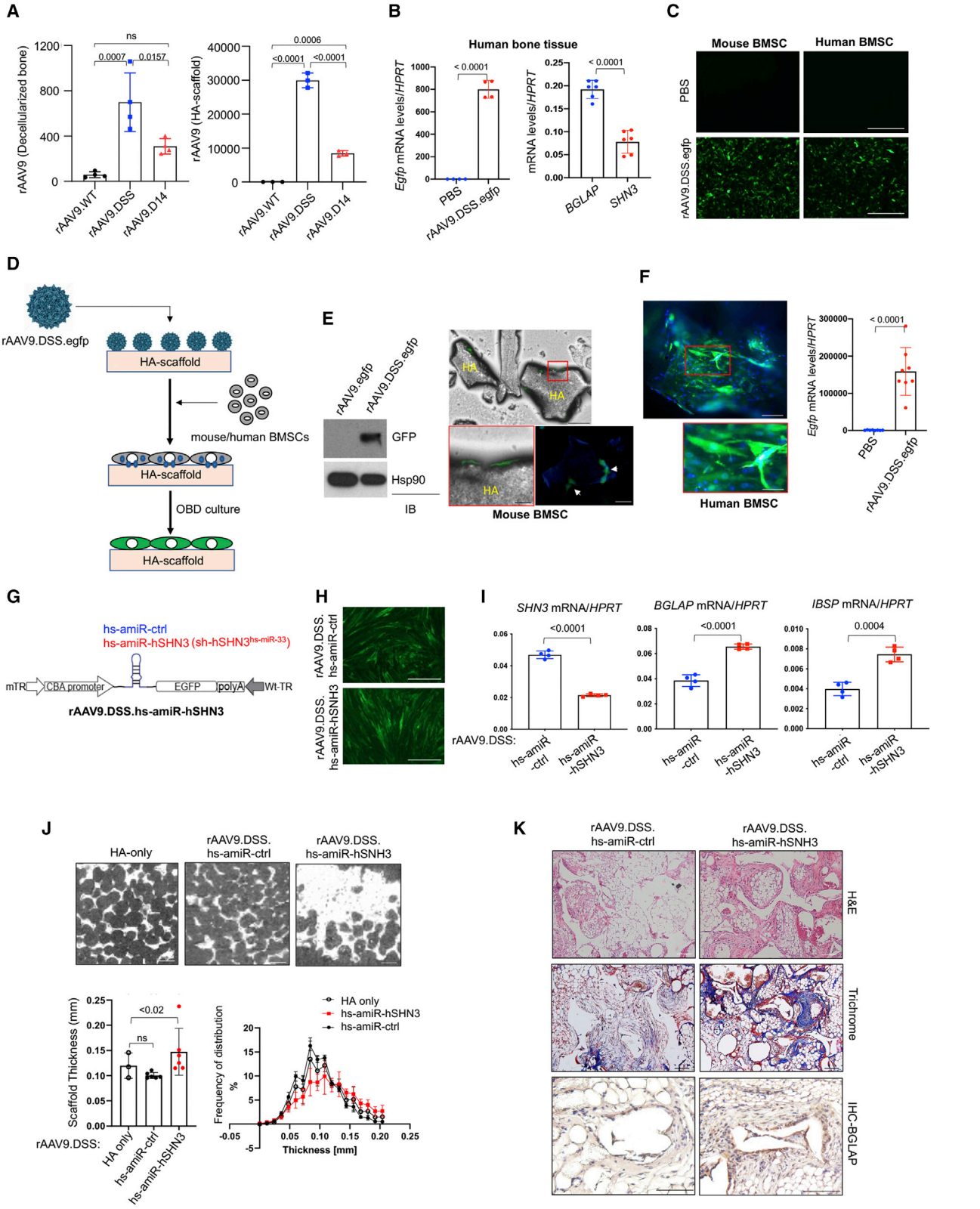

(legend on next page)

hs-amiR-hSHN3 to osteoblast-lineage cells, inducing robust bone-anabolic activity. Thus, this AAV scaffold may be useful to treat critical-sized bone defects as an optimal allograft bone with enhanced osteogenic activities.

Bone-targeted AAV gene silencers promote the healing of critical-sized bone defects

As systemic delivery of AAV gene silencers was effective for bone regeneration and fracture repair in mice, we tested their ability to promote the healing of critical-sized bone defects. A decellularized isograft obtained from background-matched WT mice was inserted into the osteotomy site of left femurs 2 weeks after i.v. injection of rAAV9.DSS carrying *amiR-ctrl*, *amiR-shn3*, *amiR-sost*, or *amiR-sost/shn3*. Twelve weeks later, bridging between the implanted isograft and host bone was assessed by radiography, microCT, and histology (Figure S11A). As seen in the fracture healing process following AAV treatment (Figures 4I–4K), *amiR-ctrl* or *amiR-sost/shn3* treatment developed persistent non-union at the osteotomy site, whereas union rates were increased by ∼60% in the presence of *amiR-shn3* or *amiR-sost* (Figures 6A, 6B, S11B, and S11C). This is accompanied with reduced numbers of TRAP-positive osteoclasts in non-union sites of the femurs treated with *amiR-sost/shn3* (Figure S11D). Thus, systemic delivery of rAAV9.DSS carrying *amiR-shn3* or *amiR-sost*, not *amiR-sost/shn3*, is effective for the healing of critical-sized bone defects as well as bone fractures.

To explore direct delivery of AAV gene silencers to osteotomy sites, a rAAV9.DSS.*egfp*-bound decellularized isograft was implanted into femoral osteotomy sites (Figure S12A). Three weeks later, the tissue distribution of AAV transduction was monitored by IVIS-100 optical imaging and fluorescence microscopy. Unlike systemic injection of an rAAV9.*egfp* showing GFP expression in the heart, liver, and muscle, little to no expression in these tissues was detected after implantation of the rAAV9.DSS.*egfp*-attached isograft (Figures 6C, 6D, and S12B), indicating that this strategy effectively restricted AAV transduction to the implantation site. Fluorescence microscopy in the brain was used as a negative control. While systemically delivered rAAV9.DSS.*egfp* mainly transduced osteoblast-lineage cells in the metaphyseal area, GFP expression was only detected in the rAAV9.DSS-isograft implanted into the osteotomy site (Figure 6E). Next, we tested whether silencing of *Shn3* or *Sost* via rAAV9.DSS-bound isograft improves the healing of critical-sized bone defects. rAAV9.DSS carrying *amiR-ctrl*, *amiR-shn3*, or *amiR-sost* were attached to the decellularized isografts and then implanted into the femoral osteotomy site. Eight weeks later, union rates between the implanted isograft and host bone were assessed by microCT and histology (Figures 6F–6H and S12C). While autograft bones without decellularization showed 100% total bridging to the host bone, only ∼20% bridging was formed in *amiR-ctrl*-treated isografts, which was improved by ∼60% when implanted with *amiR-shn3*- or *amiR-sost*-treated isografts. Remarkably, this local delivery strategy was as effective as systemic delivery of AAV gene silencers. Histologic analysis confirmed newly formed bone bridging between the host bone and *amiR-shn3*- or *amiR-sost*-treated isografts or autograft bones in the osteotomy sites, while *amiR-ctrl*-treated isografts developed fibrotic tissue at the non-union sites (Figure 6H). These results demonstrate that local delivery of WNT-modulating gene silencers to the osteotomy sites using rAAV9.DSS-bound isografts promotes the healing of critical-sized skeletal defects while limiting undesirable distribution to distant tissues. Thus, the isograft bones carrying WNT-modulating gene silencers provide enhanced osteogenic capacity, which would be useful for the treatment of critical-sized bone defects. Altogether, bone-targeted AAV-mediated regulation of WNT/β-catenin signaling in osteoblast-lineage cells may be a promising therapeutic alternative that promotes bone formation to treat osteoporosis, bone fracture, and critical-sized bone defects.

DISCUSSION

Adult bone mass is determined by the balance between osteoblast-mediated bone formation and osteoclast-mediated bone resorption, and disturbances in this equilibrium that favor bone resorption result in osteoporosis, which increases the risk of osteoporosis-associated fractures.[41] However, osteoporosis remains challenging for drug development due to numerous off-target side effects, expensive antibody-based biologics, and the high burden of taking a long-term medication.[42] Current leading osteoporosis therapies that inhibit

Figure 5. Development of a human skeletal organoid with high bone-forming activity

(A) rAAV vectors (10^9 GC) were incubated with decellularized mouse bone (left) or hydroxyapatite (HA)-based scaffold (right) for h at 37°C, and unbound rAAVs were removed by centrifugation. AAV titers were measured by ddPCR and normalized to PBS control. (B) Freshly harvested human bone tissue was incubated with PBS or rAAV9.DSS.egfp (4×10^{11} GC) for 2 days, and mRNA levels of *BGLAP*, *SHN3*, and *egfp* were measured by RT-PCR and normalized to *HPRT* (n = 4–6). (C) Mouse or human BMSCs were incubated with PBS or rAAV9.DSS.egfp (5×10^6 MOI), and, 2 days later, GFP expression was assessed by fluorescence microscopy. Scale bar, 500 μm. (D) Diagram of the study and treatment methods. (E and F) rAAV9.DSS.egfp (2×10^{11} GC) were incubated with HA scaffold for 1 h, and then mouse (E) or human (F) BMSCs were seeded on the rAAV9.DSS.egfp scaffold. Two days after the culture, GFP expression was assessed by immunoblotting with an anti-GFP antibody, fluorescence microscopy, or RT-PCR (n = 8). Scale bar: (E, right top) 500 μm, (E, right bottom) 100 μm, (F, left top) 100 μm, (F, left bottom) 25 μm. (G) Diagram of the construct containing a CBA promoter, *hs-amiR-ctrl* or *hs-amiR-hSHN3 (sh-hSHN3$^{hs\text{-}miR\text{-}33}$)*, *EGFP*, mTR/Wt-TR, and *polyA*. (H and I) Two days after incubation of human BMSCs with rAAV9.DSS carrying *hs-amiR-ctrl* or *hs-amiR-hSHN3*, AAV-transduced cells were cultured under osteogenic conditions for 4 days. GFP expression and mRNA levels of *SHN3*, *BGLAP*, or *IBSP* were assessed by fluorescence microscopy (H) and RT-PCR (I, n = 4), respectively. Scale bar, 100 μm. (J and K) HA scaffold was incubated with rAAV9.DSS carrying *hs-amiR-ctrl* or *hs-amiR-hSHN3* for 1 h and then incubated with human BMSCs under osteogenic conditions for 2 days. The scaffold was implanted into the interscapular fat pads of immunodeficient SCID mice, and, 4 weeks later, bone accrual was assessed by microCT (J). Representative 2D images (J, top) and relative quantification showing bone thickness and distribution (J, bottom) of the HA scaffold are displayed (n = 5). Non-treated HA scaffold was used as a negative control (HA only, J). Alternatively, longitudinal sections of the scaffold were stained for H&E (K, top) and trichrome (K, middle) and immuno-stained for BGLAP (K, bottom). Scale bars: (J) 100 μm, (K) 100 μm. Values represent mean ± SD by an unpaired two-tailed Student's t test (B, F, I) and one-way ANOVA test (A, J).

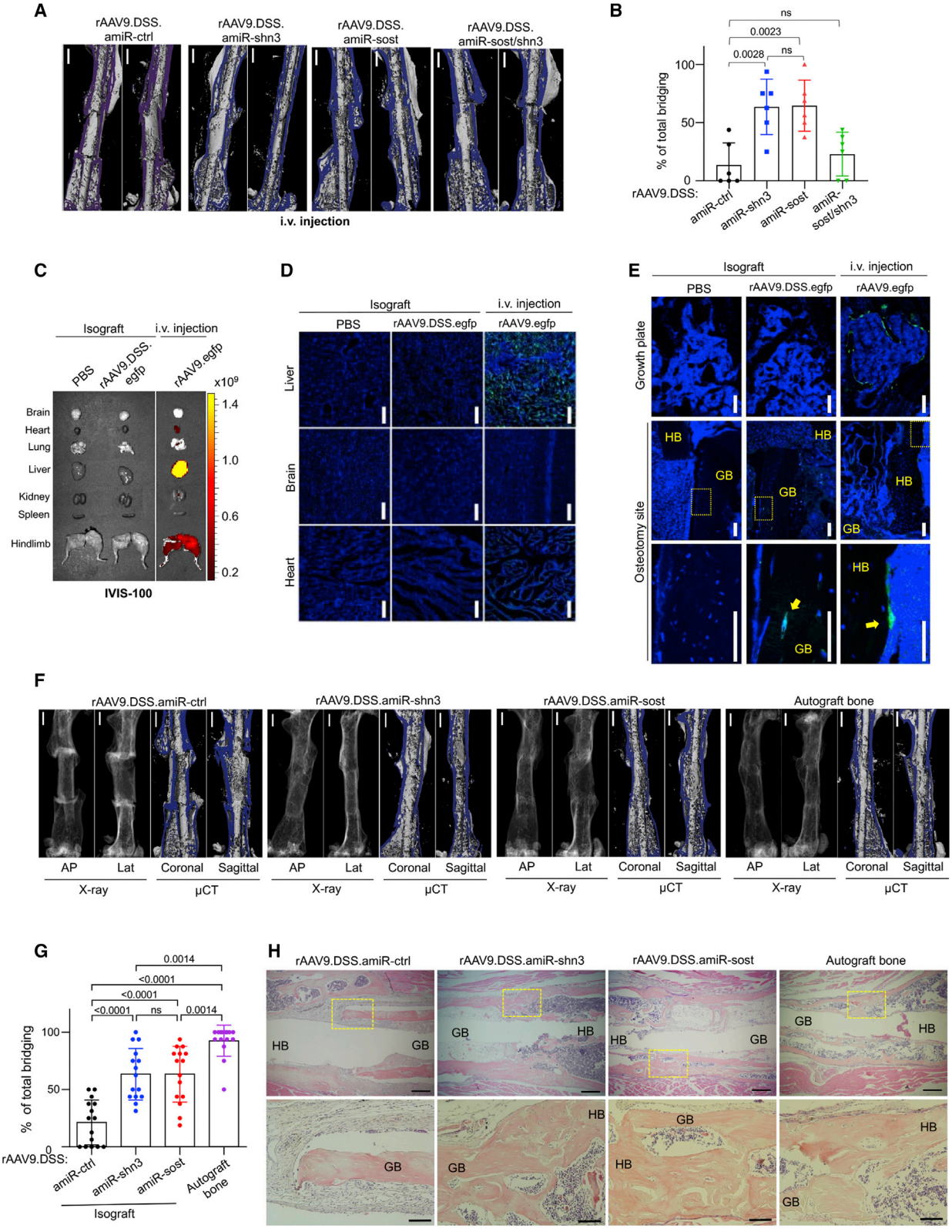

(legend on next page)

osteoclast-mediated bone resorption delay the healing of bone fractures or critical-sized bone defects due to impaired bone remodeling after long-term treatment.[2-5] Moreover, anabolic agents, including PTH, PTHrP, and anti-sclerostin antibodies, also showed minimal therapeutic effects on bone fracture or critical-sized bone defects.[43,44] Using a bone-tropic AAV targeting both secreted and intracellular WNT antagonists in osteoblast-lineage cells, this study demonstrates the potential of bone-anabolic gene therapy as an alternative approach to treat these skeletal diseases while limiting untoward off-target adverse effects in non-skeletal tissues.

With a single systemic administration, rAAV9.DSS delivered an artificial miRNA (amiR) targeting SHN3 or SOST to osteoblast-lineage cells in bone, enhanced WNT/β-catenin signaling, osteoblast function, and bone formation in models of both postmenopausal and senile osteoporosis. As the expression of *Shn3* and *Sost* is connected via a negative feedback mechanism, AAV-mediated silencing of both factors in osteoblasts further increased WNT/β-catenin signaling and osteoblast function. Remarkably, similar to the constitutive activation of β-catenin,[30] hyperactivation of canonical WNT signaling by dual silencing in osteoblasts inhibited osteoclastogenesis by upregulating *Opg* expression, counteracting bone loss in osteoporotic mice to a greater degree than that of single silencing. This effect differs from that of a single silencer treatment, which results in a mild increase in WNT/β-catenin signaling and osteoblast function without any alteration in osteoclastogenesis (Table S1). Therefore, dual silencing of *Shn3* and *Sost* via a bone-targeted AAV may be a potent combination therapy for osteoporosis.

Our AAV-mediated gene therapy has demonstrated (1) high-efficiency transduction of osteoblast-lineage cells; (2) *in vivo* targeting of single, multiple, and/or previously undruggable intracellular non-enzymatic genes; and (3) the potential to mediate long-lasting increases in bone formation after even a single systemic administration while limiting untoward off-target adverse effects in non-skeletal tissues. These properties can facilitate patient compliance, which has been identified as a key hurdle to effective osteoporosis therapy.[45] However, further development of these therapies will require consideration of the long-term durability and safety of therapeutic gene expression, as long-term suppression of bone loss will be necessary to treat osteoporosis patients. Additionally, further vector improvements to express WNT-modulating amiRs exclusively in osteoblast-lineage cells, such as using osteoblast-specific promoters or non-skeletal tissue-specific miRNA-mediated repression in the vector genome design, will enable bone-tropic rAAV vectors with even more precise bone-specific expression. Finally, future investigation for vector biodistribution, toxicity, dose-ranging, and therapeutic efficacy in non-human primates is required before any consideration can be given to applying AAV gene therapy to individuals with osteoporosis.

Critical-sized bone defects remain one of the most challenging problems in orthopedic management due to a lack of healing without any interventions, such as autograft, allograft, or synthetic bone.[36] To develop a bone-anabolic skeletal organoid for the treatment of critical-sized bone defects, we engineered a bone-targeted AAV capsid (rAAV9.DSS) that directly binds to the HA scaffold or allograft bones and efficiently transduces osteoblast-lineage cells *in vitro* and *in vivo*. Accordingly, rAAV9.DSS-bound allograft bone effectively delivered WNT-modulating amiRs to osteotomy sites, promoting critical-sized bone defect healing. Notably, a synthetic bone used in this study is a three-dimensional, HA-based scaffold that (1) contains both macropores and micropores, (2) resembles a natural structure of trabecular bone, and (3) easily recruits skeletal cells in the injured areas via high capillary effects.[39] Our previous studies show that germline deletion of *shn3* in mice[13-15] or systemic delivery of rAAV9 carrying *amiR-shn3* in mice[17] did not cause ossification or calcification of non-skeletal tissues. Here, we demonstrate that the rAAV9.DSS-bound HA scaffold carrying humanized *SHN3* amiR markedly increased the bone-forming activity of human BMSCs in xenograft mice. Altogether, these results suggest that our humanized skeletal organoid is a promising therapeutic intervention for critical-sized bone defects. Additionally, direct delivery of WNT-modulating amiRs to osteotomy sites via the rAAV9.DSS-bound bone grafts can improve therapeutic efficacy, cost-effectiveness, and safety of AAV gene therapy for critical-sized bone defects, compared with the systemic delivery of AAVs.

The WNT/β-catenin pathway is one of the most important pathways governing bone formation. Multiple mediators limiting bone formation via the inhibition of the canonical WNT pathway exist in bone, and suppression of one of them may engender a compensatory response in the other to reset WNT signaling to a steady-state. For example, treating mice with anti-sclerostin antibody upregulated expression of another secreted WNT antagonist, DKK-1. When

Figure 6. Bone-targeted AAV gene silencers promote healing of critical-sized bone defects

(A and B) Three-month-old mice were i.v. injected with rAAV9.DSS (5×10^{13} vg/kg) carrying *amiR-ctrl*, *amiR-shn3*, *amiR-sost*, or *amiR-sost/shn3* and, 2 weeks later, implantation of isograft into the osteotomy sites was performed on the left femurs. Twelve weeks later, total bridging between the implanted isograft and the host bone was assessed by microCT. Representative images (A) and percentage (B) of total bridging are displayed (n = 5–6). Scale bar: (A) 1 mm. (C–E) Decellularized isograft was incubated with PBS or rAAV9.DSS.*egfp* for 1 h, and then the PBS-treated or rAAV9.DSS.*egfp*-attached isograft was implanted into the osteotomy sites of the left femurs. Three weeks later, GFP expression in individual tissues was monitored by IVIS-100 optical imaging (C) and fluorescence microscopy (D and E). For the tissue distribution study of systemically delivered rAAV9.DSS, rAAV9.DSS.*egfp* (5×10^{13} vg/kg) was i.v. injected (n = 3). HB, host bone. Arrows indicate AAV-transduced osteoblasts. Scale bars: (D) 25 μm, (E) 100 μm. (F–H) Decellularized isograft was incubated with rAAV9.DSS (2×10^{11} GC) carrying *amiR-ctrl*, *amiR-shn3*, or *amiR-sost* for 1 h, and then rAAV9.DSS-isograft was implanted into the osteotomy sites of the left femurs. Twelve weeks later, the total bridging between the implanted isograft and the host bone was assessed by radiography and microCT (F and G). As a positive control, an autograft bone was implanted into the osteotomy sites. Representative radiography and microCT images (F), percentage of total bridging (G, n = 15), and H&E-stained longitudinal sections in the osteotomy sites (H) are displayed. Scale bars: (F) 1 mm, (H, top) 400 μm, (H, bottom) 100 μm. Values represent mean ± SD by a one-way ANOVA test (A and G).

SOST and DKK-1 were both inhibited by a bispecific antibody, bone accrual in osteoporosis and callus formation during bone fracture repair were further increased relative to treatment with anti-SOST antibody or anti-DKK-1 antibody alone.[46] Similarly, SOST expression is upregulated in the tibia lacking SHN3 (Figures 1A and 1B). Dual silencing of *Shn3* and *Sost* in osteoblast-lineage cells via a bone-targeted AAV also further increased bone mass in osteoporosis (Figures 3D–3I) and callus bone formation during fracture healing (Figure S7F). However, similar to the constitutive activation of β-catenin,[35] dual silencer treatment induced hyperactivation of WNT/β-catenin signaling, inhibited osteoclastogenesis by upregulating *Opg* expression, and exhausted osteoblast activity. This effect resulted in a delay of bone fracture healing due to reduced bone modeling activity. On the other hand, a mild increase in WNT/β-catenin signaling by single inhibition of SHN3 or SOST promoted osteogenesis without altering osteoclastogenesis, allowing bone remodeling to remain largely intact. Under this condition, the healing of bone fractures or critical-sized bone defects was substantially improved, while osteoporosis was reversed. Thus, WNT/β-catenin signaling thresholds need to be finely tuned to maximize the therapeutic effectiveness of WNT-targeting drugs. We note that, while we demonstrate SOST and SHN3 as WNT feedback regulators in this study, other WNT antagonists showing compensatory increases in expression are likely to contribute to this negative feedback mechanism.

In summary, systemic and local delivery of WNT-modulating gene silencers via a bone-targeted AAV effectively control WNT/β-catenin signaling thresholds in osteoblast-lineage cells, indicating their potential as treatments for osteoporosis, impaired bone fracture healing, and critical-sized bone defects. The potential of the bone-targeted, rAAV9-mediated therapy also extends beyond these skeletal diseases to rare skeletal disorders, where the ability of AAV-delivered payloads to correct gene mutations offers one of the only methods that can directly address the genetic defects underlying these disorders.

MATERIALS AND METHODS

Cell lines, plasmids, and antibodies

HEK293 or C2H10T1/2 cells were purchased from ATCC and grown in DMEM (Corning) supplemented with 10% FBS (Corning), 2 mM L-glutamine (Corning), 1% nonessential amino acids (Corning), and 1% penicillin/streptomycin (Corning). Ocy454 osteocytic cells were obtained from Dr. Paola Divieti Pajevic at Massachusetts General Hospital (MGH, Boston, MA) and maintained in α-MEM medium (Corning) supplemented with 10% FBS (Corning) and 1% penicillin/streptomycin (Corning) at 33°C with 5% CO_2. For osteocyte differentiation, cells were transferred to 37°C when they were confluent at 33°C and cultured for 6–12 days for the analysis of osteocyte gene expression.[28] Full-length or truncated mutants of murine *Shn3* cDNAs were PCR amplified and cloned into the pHASE/PGK-PURO lentiviral vector.[13] The human SHN3 shRNA sequence was cloned into the pLK0.1 lentiviral vector. Antibodies specific to FLAG (Sigma, F1804), HSP90α/β (BioLegend, 675402), GAPDH (EMD Millipore, CB1001), and GFP (Takara, 632381) were used. The HA-based scaffold was kindly gifted from Osteogene Tech.

rAAV vector design and production

Bone-targeted AAV9 (rAAV9.DSS, rAAV9.D14) vectors were generated as described in previous studies.[17,23] DNA sequences for *amiR-ctrl*, *amiR-sost* (*sh-mSost*$^{mmu\text{-}miR-33}$), *amiR-shn3* (*sh-mShn3*$^{mmu\text{-}miR-33}$), *hs-amiR-shn3* (*sh-mShn3*$^{hs\text{-}miR-33}$), *hs-amiR-hSHN3* (*sh-hShn3*$^{hs\text{-}miR-33}$), and *amiR-sost/hs-amiR-shn3* (*sh-mSost*$^{mmu\text{-}miR-33}$;*sh-mShn3*$^{hs\text{-}miR-33}$ were synthesized as gBlocks, cloned into the intronic region of the pAAVsc-*CB6-Egfp* plasmid at the restriction enzyme sites (PstI and BglII),[47] and packaged into the AAV9.DSS capsid. rAAV production was performed by transient transfection of HEK293 cells, purified by CsCl sedimentation, and titered by droplet digital PCR (ddPCR) on a QX200 ddPCR system (Bio-Rad) using the Egfp prime/probe set as previously described.[48] The sequences of gBlocks and oligonucleotides for ddPCR are listed in Table S2.

Mice

Shn3$^{-/-}$[14] and *Shn3*$^{fl/fl}$[49] mice were previously generated and maintained on BALB/c and C57BL/6J background, respectively. WT C57BL/6J, severe combined immunodeficiency (SCID), and TCF/Lef1-HIST1H2BB/EGFP mice were purchased from the Jackson Laboratory. Mouse genotypes were determined by PCR on tail genomic DNA; primer sequences are available upon request. All animals were used in accordance with the NIH Guide for the Care and Use of Laboratory Animals and were handled according to protocols approved by the University of Massachusetts Chan Medical School Institutional Animal Care and Use Committee (under protocol A-2564).

MicroCT analysis

MicroCT was used for qualitative and quantitative assessment of trabecular and cortical bone microarchitecture and performed by an investigator blinded to the genotypes of the animals under analysis. Femurs excised from the indicated mice were fixed with 10% neutral buffered formalin and scanned using a microCT 35 (Scanco Medical) with a spatial resolution of 7 μm. For trabecular bone analysis of the distal femur, an upper 2.1-mm region beginning 280 μm proximal to the growth plate was contoured. For cortical bone analysis of the femur, a midshaft region of 0.6 mm in length was used. MicroCT scans of L4 spinal segments were performed using isotropic voxel sizes of 12 μm. 3D reconstruction images were obtained from contoured 2D images by methods based on distance transformation of the binarized images. Alternatively, the Inveon multimodality 3D visualization program was used to generate a fused 3D viewing of multiple static or dynamic volumes of microCT modalities (Siemens Medical Solutions USA). All images presented are representative of the respective genotypes ($n > 5$).

Histology, histomorphometry, and immunofluorescence

For histological analysis, femurs were dissected from the mice treated with rAAVs, fixed in 10% neutral buffered formalin for 2 days, and decalcified by 5% tetrasodium EDTA for 2–4 weeks. Tissues were dehydrated by passage through an ethanol series, cleared twice in xylene, embedded in paraffin, and sectioned at a thickness of 6 μm along the coronal plane from anterior to posterior. Decalcified femoral sections were stained with hematoxylin and eosin (H&E), TRAP, or trichrome.

For dynamic histomorphometry analysis, 25 mg/kg calcein (Sigma, C0875) and 50 mg/kg alizarin-3-methyliminodiacetic acid (Sigma, A3882) dissolved in 2% sodium bicarbonate solution were administered via subcutaneous (s.c.) injection into mice at 6-day intervals. After fixation in 10% neutral buffered formalin for 2 days, undecalcified femur samples were embedded in methylmethacrylate, and the proximal metaphysis was sectioned longitudinally (5 μm) and stained with McNeal's trichrome for osteoid assessment, toluidine blue for osteoblasts, and TRAP for osteoclasts.[50] A region of interest was defined, and the following ratios were measured using a Nikon Optiphot 2 microscope interfaced to a semiautomatic analysis system (Osteometrics): bone-formation rate (BFR)/bone surface (BS), MAR, osteoblast surface (OB.S)/BS, osteoblast number (OB.N)/BS, osteoclast surface (OC.S)/BS, osteoclast number (OC.N)/bone perimeter (B.Pm), and erosion surface (ES)/BS. Measurements were taken on two sections/sample (separated by ~25 μm) and summed prior to normalization to obtain a single measure/sample in accordance with American Society for Bone and Mineral Research standards.[51] This methodology has undergone extensive quality control and validation, and the results were assessed by two different researchers in a blinded fashion.

For immunofluorescence, fresh femurs and vertebrae dissected from rAAV-treated mice were collected and immediately fixed in ice-cold 4% paraformaldehyde solution for 2 days. Semi-decalcification was carried out for 5 days in 0.5 M EDTA pH 7.4 at 4°C with constant shaking (age $\geq$ 1 week), and infiltration was followed with a mixture of 20% sucrose phosphate buffer for 1 day and a 25% sucrose phosphate buffer the subsequent day. All samples were embedded in a 50/50 mixture of 25% sucrose solution and OCT compound (Sakura) and cut into 12-μm-thick sagittal sections using a cryostat (Leica). Immunofluorescence staining and analysis was performed as described previously.[50,52] Briefly, after treatment with 0.2% Triton X-100 for 10 min, sections were blocked with 5% donkey serum at room temperature for 30 min and incubated overnight at 4°C with an anti-BGLAP antibody (sc-365797, Santa Cruz, 1:150) or anti-SOST antibody (AF 1589, R&D systems, 1:100). Primary antibodies were visualized with donkey anti-rat IgG Alexa 594 (1:500, Molecular Probes). Nuclei were counterstained with DAPI. An Olympus IX81 confocal microscope or Leica TCS SP5 II Zeiss LSM-880 confocal microscope was used to image samples.

Luciferase reporter assay

The AAV-treated Ocy454 osteocyte line was transfected with a β-catenin-responsive reporter gene (Top-flash Luc) using the Effectene transfection reagent (Qiagen) and cultured for 6 days in the presence of recombinant WNT3a (25 μg/mL, R&D Systems). A luciferase assay was performed according to the manufacturer's protocol (Promega).

Quantitative RT-PCR analysis

Total RNA was purified from cells using QIAzol (QIAGEN), and cDNA was synthesized using the High-Capacity cDNA Reverse Transcription Kit from Applied Biosystems. Quantitative RT-PCR was performed using SYBR Green PCR Master Mix (Bio-Rad) with CFX connect RT-PCR detection system (Bio-Rad). To measure mRNA levels in bone tissues, after removal of bone marrow, tibias were snap-frozen in liquid nitrogen for 30 s and homogenized in 1 mL of QIAzol for 1 min. Primers used for PCR are described in Table S2.

Immunoblotting analysis

Cells were lysed in TNT lysis buffer(50 mM Tris-HCl [pH 7.4], 150 mM NaCl, 1% Triton X-100, 1 mM EDTA, 1 mM EGTA, 50 mM NaF, 1 mM Na_3VO_4, 1 mM PMSF, and protease inhibitor cocktail [Sigma]), and protein amounts from cell lysates were measured using the DC protein assay (Bio-Rad). Equivalent amounts of protein were subjected to SDS-PAGE, transferred to Immobilon-P PVDF membranes (Millipore), immunoblotted with the indicated antibodies, and developed with enhanced chemiluminescence (ECL) (Thermo Fisher Scientific). Immunoblotting with an anti-HSP90 antibody was used as a loading control.

Effects of AAV-mediated delivery of WNT-modulating gene silencers on bone formation

Two-month-old WT mice were injected i.v. with a single dose of rAAV9.DSS carrying *amiR-ctrl*, *hs-amiR-shn3*, *or amiR-shn3* (5×10^{13} vg/kg, 200 μL), and 2 months later the knockdown efficiency of *Shn3* in the tibia and femoral bone mass was assessed by RT-PCR and microCT, respectively. Two-month-old TCF/Lef1-GFP reporter mice were injected i.v. with a single dose of rAAV9.DSS (5×10^{13} vg/kg, 200 μL) carrying *mCherry*, *amiR-ctrl*, or *amiR-sost/shn3* and, 2 weeks later, tibias were subjected to RT-PCR and immunoblotting analyses, and femoral bones were subjected to radiography and microCT. Two-month-old WT mice were injected i.v. with a single dose of rAAV9.DSS (5×10^{13} vg/kg, 200 μL) carrying *amiR-ctrl*, *amiR-sost*, *amiR-shn3*, or *amiR-sost/shn3* and, 3 weeks later, mice were injected s.c. with calcein and alizarin-3-methyliminodiacetic acid at 4-day intervals for dynamic histomorphometry analysis. Non-labeled mice were used to monitor GFP expression using the IVIS-100 optical imaging or cryo-sections.

Effects of AAV-mediated delivery of WNT-modulating gene silencers on osteoporosis

Mouse models of postmenopausal osteoporosis were generated by anesthetizing and bilaterally ovariectomizing 3-month-old female mice (The Jackson Laboratory). Six weeks after surgery, sham or OVX mice were injected i.v. with a single dose of rAAV9.DSS (5×10^{13} vg/kg, 200 μL) carrying *amiR-ctrl*, *amiR-sost*, *amiR-shn3*, or *amiR-sost/shn3*. Mice were randomly divided into five groups (sham + rAAV9.DSS-*amiR-ctrl*, OVX + rAAV9-*amiR-ctrl*, OVX + rAAV9-*amiR-shn3*, OVX + rAAV9.DSS.*amiR-sost*, OVX + rAAV9.DSS.*amiR-sost/shn3*). Eight weeks after the injection, mice were injected s.c. with calcein and alizarin-3-methyliminodiacetic acid at 6-day intervals for dynamic histomorphometric analysis. Non-labeled mice were used to monitor GFP expression using the IVIS-100 optical imaging or cryo-sections. As a mouse model of senile osteoporosis, 20-month-old male mice were injected i.v. with a single dose of rAAV9.DSS (5×10^{13} vg/kg, 200 μL) and, 2 months later, bone mass in the femurs and lumbar vertebrae (L4) was assessed by microCT.

Effects of AAV-mediated delivery of WNT-modulating gene silencers on the healing of uni-cortical bone defects

A single dose of rAAV9.DSS (5×10^{13} vg/kg, 200 μL) carrying *amiR-ctrl*, *amiR-shn3*, *amiR-sost*, or *amiR-sost/shn3* was i.v. injected into 2-month-old female mice 2 weeks before the surgery. The uni-cortical bone defect was conducted under general anesthesia (isoflurane, 1%–4%), and the pain was controlled by s.c. injection of buprenorphine (0.03 mg/kg) 1 h before surgery. Mice were placed in the lateral decubitus position, and the surgical site was prepared with disinfection and draped with a surgical cloth. A 1.0-cm skin incision was made on the lateral aspect of the femur, and the femur was exposed by accessing it through the vastus lateralis. A bone defect with a length of 3 mm and a width of 1 mm was made using a 1-mm motorized burr while protecting the posterior femoral nerve. The defect site was irrigated with PBS to remove a bone fragment within the medulla, and the fascia and skin were closed with the Vicryl 4/0 and nylon 5/0. 2 weeks after the surgery, fluorescence microscopy and RT-PCR analysis on the tibial bone RNA were performed to assess AAV's transduction and knockdown efficiency, respectively. Skeletal analyses were performed using microCT and histology.

Effects of AAV-mediated delivery of WNT-modulating gene silencers on bone fracture healing

A single dose of rAAV9.DSS (5×10^{13} vg/kg, 200 μL) carrying *amiR-ctrl*, *amiR-shn3*, *amiR-sost*, or *amiR-sost/shn3* was i.v. injected into 12-week-old male mice 2 weeks before the surgery. Mice were placed in a lateral recumbent position and covered with a sterile surgical drape. A longitudinal skin incision was made along the lateral aspect of the thigh from the stifle joint to the hip. The lateral aspect of the femur was exposed by parting the vastus lateralis muscle and the rectus femoris muscle to expose the length of the femur while preserving the femoral nerve. The middle of the femoral shaft was excised with a surgical saw. Intramedullary fixation was performed with a 25G needle penetrating from the patella furrow of the distal femur to the greater trochanter tip of the femur. Both ends of the needle were bent and then cut with a wire cutter, leaving 1 mm. The fascia was sutured using a 4/0 Vicryl suture, and then the skin was closed using a 4/0 nylon suture. Radiography of the injured legs was performed to monitor fracture healing 2 weeks post surgery. Four weeks later, fluorescence microscopy and RT-PCR analysis on tibial RNA were performed to assess AAV's transduction and knockdown efficiency, respectively. MicroCT and histology were performed for skeletal analyses. Fracture union rates were defined as all bony bridges observed between the ends of fractured cortical bones in coronal and sagittal reconstruction views of microCT.

Effects of AAV-mediated delivery of WNT-modulating gene silencers on human skeletal organoid in xenograft mice

HA scaffold (Osteogene Tech) was incubated with rAAV9.DSS (2×10^{11} GC) carrying *hs-amiR-ctrl* or *hs-amiR-hSHN3* for 1 h at 37°C, and unbound rAAV9.DSS vectors were removed by centrifugation. Human BMSCs on the AAV-attached scaffold were cultured under osteogenic conditions for 2 days, then implanted into the interscapular fat pads of 3-month-old immunodeficient SCID mice. Four weeks later, bone formation was assessed by microCT and histology. Mature osteoblasts on the implanted scaffold were assessed by IHC for BGLAP.

Effects of AAV-mediated delivery of WNT-modulating gene silencers on critical-sized bone defects

A single dose of rAAV9.DSS (5×10^{13} vg/kg, 200 μL) carrying *amiR-ctrl*, *amiR-shn3*, *amiR-sost*, or *amiR-sost/shn3* were i.v. injected into 3-month-old mice 2 weeks before the surgery. Allogenous femoral bone graft was obtained from mice of the same age and sex, prepared by decellularization using sonication, and stored at −80°C. Mice were placed in a lateral recumbent position and covered with a sterile surgical drape. A longitudinal 2.0-cm skin incision was made along the lateral aspect of the thigh from the stifle joint to the hip. The femur shaft was exposed by dissecting the muscle fascia slightly anterior to the lateral intermuscular septum while protecting the neurovascular bundle located posteriorly. To make the bone defect artificially, osteotomy of the femur (4-mm length) was conducted with the oscillating saw. Then the allogenous femoral bone graft (thawed in cold PBS) was inserted into the gap site, and the 23G needle was passed through the medulla of femoral bone and allogenous bone to fix entire surgical structures. After irrigating the operation site with PBS to remove a bone fragment from the muscle or other soft tissue, the fascia and skin were closed with the Vicryl 4/0 and nylon 5/0. Twelve weeks after the surgery, skeletal analyses were performed using microCT and histology.

Alternatively, an allogenous femoral bone graft was incubated with rAAV9.DSS (2×10^{11} GC) carrying *amiR-ctrl*, *amiR-shn3*, or *amiR-sost* for 1 h at 37°C, and unbound rAAV9.DSS vectors were removed by centrifugation. Implantation of isograft into the osteotomy sites was performed in 3-month-old mice, and, 12 weeks later, skeletal analyses were performed using microCT and histology. An autogenous bone graft obtained from the same mice was implanted into the osteotomy sites without decellularization as a positive control. Bridging between a bone graft and host bone was assessed at four corners of grafted bone on two sets of orthogonal longitudinal image pairs in microCT, which captured bridging every 45° around the circumference of the bone. For each image, two blind observers scored the presence of a bony bridge on each of four corners, with the results averaged and expressed as a percentage of the total bridging for each sample.

Statistics and reproducibility

All experiments were carried out at least two or three times. For IHC, histological staining, and immunoblotting, representative images are shown. All data are shown as the mean ± standard deviation (SD). We first performed the Shapiro-Wilk normality test to check for normal distributions of the groups. For comparisons between two groups, a two-tailed, unpaired Student's t test was used if normality tests were passed, and, if normality tests failed, the Mann-Whitney tests were used. For comparisons among three or four groups, we used one-way ANOVA if normality tests passed, followed by Tukey's multiple comparison test for all pairs of groups. The GraphPad PRISM

software (version 9.0.0, La Jolla, CA) was used for statistical analysis. $p < 0.05$ was considered statistically significant.

DATA AND MATERIALS AVAILABILITY

Data and materials supporting the findings of this manuscript are available from the corresponding authors upon reasonable request.

SUPPLEMENTAL INFORMATION

Supplemental information can be found online at https://doi.org/10.1016/j.ymthe.2022.09.018.

ACKNOWLEDGMENTS

We thank Dr. Laurie Glimcher (Department of Cancer Immunology and Virology, Dana Farber Cancer Institute and Harvard Medical School) for providing *Schnurri-3* knockout and floxed mice; Tadatoshi Sato, Ji-Hea Kim, Ok-sun Lee, Zhihao Chen, and Eunhye Son for providing technical support; and Drs. Merin MacDonald and Melanie Trombly for reviewing the manuscript. We also thank the many individuals who provided valuable reagents. G.G. is supported by grants from the NIH (P01AI100263, R01NS076991, P01HD080642, R01AI12135). J.-H.S. is supported by NIH/NIAMS (R21AR077557, R01AR078230), the International FOP Association, and AAVAA Therapeutics. M.B.G. is supported by NIH/NIAMS (R01AR075585), a Career Award for Medical Scientists from the Burroughs Wellcome Fund, and the Pershing Square Sohn Cancer Research Alliance.

AUTHOR CONTRIBUTIONS

W.-T.O. and Y.-S.Y. designed, executed, and interpreted the experiments. J.X. and H.M. designed and generated all of the AAVs used in this work. J.-M.K., K.-H.P.-M., and K.-H.P. performed the ovariectomies and AAV transduction to human bone tissue. D.S.O. provided the HA scaffold. M.B.G. supervised the research and manuscript. G.G. and J.-H.S. supervised the research and prepared the manuscript. All authors revised the manuscript and approved the final draft.

DECLARATION OF INTERESTS

J.-H.S. is a scientific co-founder of AAVAA Therapeutics and holds equity in this company. G.G. is a scientific co-founder of AAVAA Therapeutics, Voyager Therapeutics, and Aspa Therapeutics and holds equity in these companies. G.G. is an inventor on patents with potential royalties licensed to Voyager Therapeutics, Aspa Therapeutics, and other biopharmaceutical companies. D.S.O. is a chief scientific officer of Osteogene Tech. These pose no conflicts for this study. The other authors declare no competing interests.

REFERENCES

1. Langdahl, B., Ferrari, S., and Dempster, D.W. (2016). Bone modeling and remodeling: potential as therapeutic targets for the treatment of osteoporosis. Ther. Adv. Musculoskelet. Dis. *8*, 225–235.
2. Eastell, R., Christiansen, C., Grauer, A., Kutilek, S., Libanati, C., McClung, M.R., et al. (2011). Effects of denosumab on bone turnover markers in postmenopausal osteoporosis. J. Bone Miner Res. *26*, 530–537.
3. Rasmusson, L., and Abtahi, J. (2014). Bisphosphonate associated osteonecrosis of the jaw: an update on pathophysiology, risk factors, and treatment. Int. J. Dent *2014*, 471035.
4. Gerstenfeld, L.C., Sacks, D.J., Pelis, M., Mason, Z.D., Graves, D.T., Barrero, M., et al. (2009). Comparison of effects of the bisphosphonate alendronate versus the RANKL inhibitor denosumab on murine fracture healing. J. Bone Miner Res. *24*, 196–208.
5. Russow, G., Jahn, D., Appelt, J., Mardian, S., Tsitsilonis, S., and Keller, J. (2018). Anabolic therapies in osteoporosis and bone regeneration. Int. J. Mol. Sci. *20*.
6. Augustine, M., and Horwitz, M.J. (2013). Parathyroid hormone and parathyroid hormone-related protein analogs as therapies for osteoporosis. Curr. Osteoporos. Rep. *11*, 400–406.
7. Esbrit, P., and Alcaraz, M.J. (2013). Current perspectives on parathyroid hormone (PTH) and PTH-related protein (PTHrP) as bone anabolic therapies. Biochem. Pharmacol. *85*, 1417–1423.
8. Kraenzlin, M.E., and Meier, C. (2011). Parathyroid hormone analogues in the treatment of osteoporosis. Nat. Rev. Endocrinol. *7*, 647–656.
9. Appelman-Dijkstra, N.M., and Papapoulos, S.E. (2018). Clinical advantages and disadvantages of anabolic bone therapies targeting the WNT pathway. Nat. Rev. Endocrinol. *14*, 605–623.
10. Holdsworth, G., Roberts, S.J., and Ke, H.Z. (2019). Novel actions of sclerostin on bone. J. Mol. Endocrinol. *62*, R167–R185.
11. McClung, M.R., Grauer, A., Boonen, S., Bolognese, M.A., Brown, J.P., Diez-Perez, A., et al. (2014). Romosozumab in postmenopausal women with low bone mineral density. N. Engl. J. Med. *370*, 412–420.
12. Bovijn, J., Krebs, K., Chen, C.Y., Boxall, R., Censin, J.C., Ferreira, T., et al. (2020). Evaluating the cardiovascular safety of sclerostin inhibition using evidence from meta-analysis of clinical trials and human genetics. Sci. Transl Med. *12*.
13. Shim, J.H., Greenblatt, M.B., Zou, W., Huang, Z., Wein, M.N., Brady, N., et al. (2013). Schnurri-3 regulates ERK downstream of WNT signaling in osteoblasts. J. Clin. Invest. *123*, 4010–4022.
14. Jones, D.C., Wein, M.N., Oukka, M., Hofstaetter, J.G., Glimcher, M.J., and Glimcher, L.H. (2006). Regulation of adult bone mass by the zinc finger adapter protein Schnurri-3. Science *312*, 1223–1227.
15. Wein, M.N., Jones, D.C., Shim, J.H., Aliprantis, A.O., Sulyanto, R., Lazarevic, V., et al. (2012). Control of bone resorption in mice by Schnurri-3. Proc. Natl. Acad. Sci. USA *109*, 8173–8178.
16. Xu, R., Yallowitz, A., Qin, A., Wu, Z., Shin, D.Y., Kim, J.M., et al. (2018). Targeting skeletal endothelium to ameliorate bone loss. Nat. Med. *24*, 823–833.
17. Yang, Y.S., Xie, J., Wang, D., Kim, J.M., Tai, P.W.L., Gravallese, E., et al. (2019). Bone-targeting AAV-mediated silencing of Schnurri-3 prevents bone loss in osteoporosis. Nat. Commun. *10*, 2958.
18. Hofstaetter, J.G., Misof, B.M., Jones, D.C., Zoehrer, R., Blouin, S., Schueler, C., et al. (2019). Biomechanical and bone material properties of schnurri-3 Null mice. JBMR Plus *3*, e10226.
19. Bulcha, J.T., Wang, Y., Ma, H., Tai, P.W.L., and Gao, G. (2021). Viral vector platforms within the gene therapy landscape. Signal Transduct Target Ther. *6*, 53.
20. Wang, D., Tai, P.W.L., and Gao, G. (2019). Adeno-associated virus vector as a platform for gene therapy delivery. Nat. Rev. Drug Discov. *18*, 358–378.
21. MacNabb, C., Patton, D., and Hayes, J.S. (2016). Sclerostin antibody therapy for the treatment of osteoporosis: clinical Prospects and Challenges. J. Osteoporos. *2016*, 6217286.
22. Canalis, E. (2013). Wnt signalling in osteoporosis: mechanisms and novel therapeutic approaches. Nat. Rev. Endocrinol. *9*, 575–583.
23. Yang, Y.S., Xie, J., Chaugule, S., Wang, D., Kim, J.M., Kim, J., et al. (2020). Bone-targeting AAV-mediated gene silencing in osteoclasts for osteoporosis therapy. Mol. Ther. Methods Clin. Dev. *17*, 922–935.
24. Grimm, D., Streetz, K.L., Jopling, C.L., Storm, T.A., Pandey, K., Davis, C.R., et al. (2006). Fatality in mice due to oversaturation of cellular microRNA/short hairpin RNA pathways. Nature *441*, 537–541.
25. McBride, J.L., Boudreau, R.L., Harper, S.Q., Staber, P.D., Monteys, A.M., Martins, I., et al. (2008). Artificial miRNAs mitigate shRNA-mediated toxicity in the brain: implications for the therapeutic development of RNAi. Proc. Natl. Acad. Sci. USA *105*, 5868–5873.

26. Xie, J., Tai, P.W.L., Brown, A., Li, C., Zamore, P.D., and Gao, G. (2018). A Novel rAAV-amiRNA Platform Enables Potent in Vivo Gene Silencing and a Ten-fold Enhancement of On-Target Specificity over Conventional shRNA Vectors (American Society of Gene and Cell Therapy 21st Annual Meeting).
27. D'Onofrio, D.J., and Abel, D.L. (2014). Redundancy of the genetic code enables translational pausing. Front Genet. *5*, 140.
28. Spatz, J.M., Wein, M.N., Gooi, J.H., Qu, Y., Garr, J.L., Liu, S., et al. (2015). The Wnt inhibitor sclerostin is up-regulated by mechanical Unloading in osteocytes in vitro. J. Biol. Chem. *290*, 16744–16758.
29. Ferrer-Vaquer, A., Piliszek, A., Tian, G., Aho, R.J., Dufort, D., and Hadjantonakis, A.K. (2010). A sensitive and bright single-cell resolution live imaging reporter of Wnt/ss-catenin signaling in the mouse. BMC Dev. Biol. *10*, 121.
30. Glass, D.A., 2nd, Bialek, P., Ahn, J.D., Starbuck, M., Patel, M.S., Clevers, H., et al. (2005). Canonical Wnt signaling in differentiated osteoblasts controls osteoclast differentiation. Dev. Cell *8*, 751–764.
31. Nakamura, T., Imai, Y., Matsumoto, T., Sato, S., Takeuchi, K., Igarashi, K., et al. (2007). Estrogen prevents bone loss via estrogen receptor alpha and induction of Fas ligand in osteoclasts. Cell *130*, 811–823.
32. Bouxsein, M.L., Myers, K.S., Shultz, K.L., Donahue, L.R., Rosen, C.J., and Beamer, W.G. (2005). Ovariectomy-induced bone loss varies among inbred strains of mice. J. Bone Miner Res. *20*, 1085–1092.
33. Windolf, M., Ernst, M., Schwyn, R., Arens, D., and Zeiter, S. (2021). The relation between fracture activity and bone healing with special reference to the early healing phase - a preclinical study. Injury *52*, 71–77.
34. Hulsart-Billstrom, G., Bergman, K., Andersson, B., Hilborn, J., Larsson, S., and Jonsson, K.B. (2015). A uni-cortical femoral defect model in the rat: evaluation using injectable hyaluronan hydrogel as a carrier for bone morphogenetic protein-2. J. Tissue Eng. Regen. Med. *9*, 799–807.
35. Bao, Q., Chen, S., Qin, H., Feng, J., Liu, H., Liu, D., et al. (2017). An appropriate Wnt/beta-catenin expression level during the remodeling phase is required for improved bone fracture healing in mice. Sci. Rep. *7*, 2695.
36. Baldwin, P., Li, D.J., Auston, D.A., Mir, H.S., Yoon, R.S., and Koval, K.J. (2019). Autograft, allograft, and bone graft Substitutes: clinical evidence and indications for Use in the setting of Orthopaedic Trauma surgery. J. Orthop. Trauma *33*, 203–213.
37. Zhang, G., Guo, B., Wu, H., Tang, T., Zhang, B.T., Zheng, L., et al. (2012). A delivery system targeting bone formation surfaces to facilitate RNAi-based anabolic therapy. Nat. Med. *18*, 307–314.
38. Ogawa, K., Ishizaki, A., Takai, K., Kitamura, Y., Makino, A., Kozaka, T., et al. (2017). Evaluation of Ga-DOTA-(D-Asp)n as bone imaging agents: D-aspartic acid peptides as carriers to bone. Sci. Rep. *7*, 13971.
39. Oh, D.S., Koch, A., Eisig, S., Kim, S.G., Kim, Y.H., Kim, D.G., et al. (2015). Distinctive capillary action by Micro-channels in bone-like Templates can enhance Recruitment of cells for Restoration of large bony defect. J. Vis. Exp.
40. Oukka, M., Kim, S.T., Lugo, G., Sun, J., Wu, L.C., and Glimcher, L.H. (2002). A mammalian homolog of Drosophila schnurri, KRC, regulates TNF receptor-driven responses and interacts with TRAF2. Mol. Cell *9*, 121–131.
41. Harada, S., and Rodan, G.A. (2003). Control of osteoblast function and regulation of bone mass. Nature *423*, 349–355.
42. Li, S.-S., He, S.-H., Xie, P.-Y., Li, W., Zhang, X.-X., Li, T.-F., et al. (2021). Recent Progresses in the treatment of osteoporosis. Front. Pharmacol. *12*.
43. Morse, A., McDonald, M.M., Schindeler, A., Peacock, L., Mikulec, K., Cheng, T.L., et al. (2017). Sclerostin antibody increases callus size and Strength but does not improve fracture union in a challenged open rat fracture model. Calcif Tissue Int. *101*, 217–228.
44. Yukata, K., Kanchiku, T., Egawa, H., Nakamura, M., Nishida, N., Hashimoto, T., et al. (2018). Continuous infusion of PTH1-34 delayed fracture healing in mice. Sci. Rep. *8*, 13175.
45. Khosla, S., and Shane, E. (2016). A Crisis in the treatment of osteoporosis. J. Bone Miner Res. *31*, 1485–1487.
46. Florio, M., Gunasekaran, K., Stolina, M., Li, X., Liu, L., Tipton, B., et al. (2016). A bispecific antibody targeting sclerostin and DKK-1 promotes bone mass accrual and fracture repair. Nat. Commun. *7*, 11505.
47. Xie, J., Mao, Q., Tai, P.W.L., He, R., Ai, J., Su, Q., et al. (2017). Short DNA hairpins Compromise recombinant adeno-associated virus genome Homogeneity. Mol. Ther. *25*, 1363–1374.
48. Gao, G., and Sena-Esteves, M. (2012). Introducing genes into mammalian cells: Viral vectors. Mol. Cloning *2*, 1209–1313.
49. Jones, D.C., Schweitzer, M.N., Wein, M., Sigrist, K., Takagi, T., Ishii, S., et al. (2010). Uncoupling of growth plate maturation and bone formation in mice lacking both Schnurri-2 and Schnurri-3. Proc. Natl. Acad. Sci. USA *107*, 8254–8258.
50. Fukuda, T., Takeda, S., Xu, R., Ochi, H., Sunamura, S., Sato, T., et al. (2013). Sema3A regulates bone-mass accrual through sensory innervations. Nature *497*, 490–493.
51. Parfitt, A.M., Drezner, M.K., Glorieux, F.H., Kanis, J.A., Malluche, H., Meunier, P.J., et al. (1987). Bone histomorphometry: standardization of nomenclature, symbols, and units. Report of the ASBMR Histomorphometry Nomenclature Committee. J. Bone Miner Res. *2*, 595–610.
52. Xu, R., Zhang, C., Shin, D.Y., Kim, J.M., Lalani, S., Li, N., et al. (2017). c-Jun N-terminal kinases (JNKs) are critical mediators of osteoblast activity in vivo. J. Bone Miner Res.

YMTHE, Volume *31*

Supplemental Information

WNT-modulating gene silencers as a gene therapy for osteoporosis, bone fracture, and critical-sized bone defects

Won-Taek Oh, Yeon-Suk Yang, Jun Xie, Hong Ma, Jung-Min Kim, Kwang-Hwan Park, Daniel S. Oh, Kyung-Hyun Park-Min, Matthew B. Greenblatt, Guangping Gao, and Jae-Hyuck Shim

Supplementary Materials for:

WNT-modulating gene silencers as a gene therapy for osteoporosis, bone fracture, and critical-sized bone defects

Won-Taek Oh[1,2]†, Yeon-Suk Yang[1]†, Jun Xie[3,4,5], Hong Ma[3,4,5], Jung-Min Kim[1], Kwang-Hwan Park[2], Daniel S. Oh[6], Kyung-Hyun Park-Min[7,8], Matthew B. Greenblatt[8,9], Guangping Gao[3,4,5,10]*, and Jae-Hyuck Shim[1,3,10]*

†These authors contributed equally to this work.

*Corresponding authors: Jae-Hyuck Shim. Email: jaehyuck.shim@umassmed.edu and Guangping Gao. Email: guangping.gao@umassmed.edu

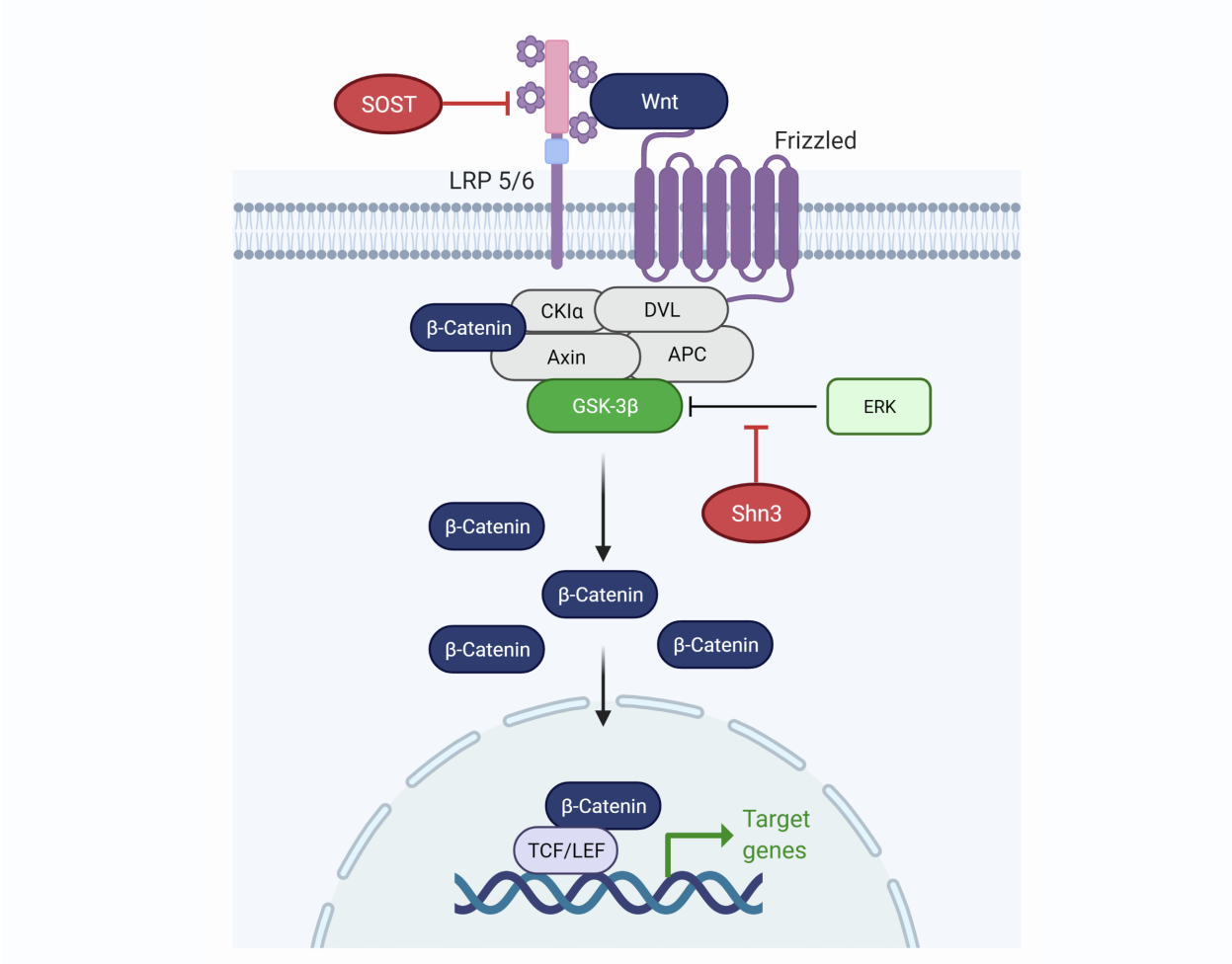

Fig. S1. Schematic diagram showing the molecular mechanism of SHN3 and SOST in the WNT/β-catenin pathway (created with biorender.com). Abbreviations: CK1α, casein kinase 1α; LRP 5/6, low-density lipoprotein receptor-related proteins 5 and 6; DVL, dishevelled; APC, adenomatous polyposis coli; GSK-3β, glycogen synthase kinase 3 beta; ERK, extracellular signal-regulated kinase; TCF/LEF, T-cell factor/lymphoid enhancer factor.

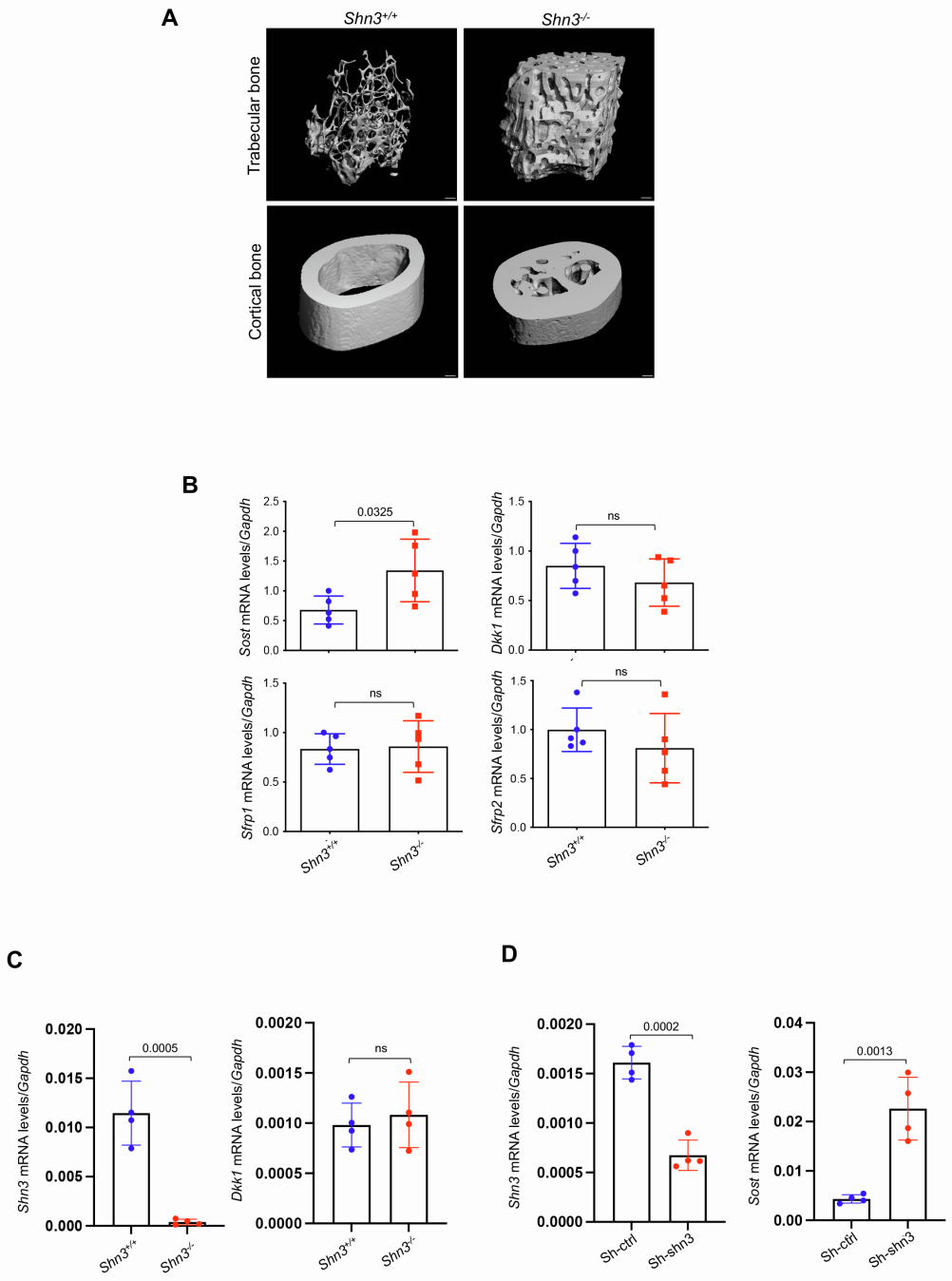

Fig. S2. Expression of secreted WNT antagonists in *Shn3*$^{-/-}$ mice.
A. MicroCT analysis showing trabecular bone mass and midshaft cortical bone thickness in femurs obtained from 2-month-old *shn3*$^{+/+}$ and *shn3*$^{-/-}$ mice. Scale bar: 200 μm. **B.** mRNA levels of secreted WNT antagonists in the tibia, *Sost, Dkk1, Sfrp1, or Sfrp2,* were measured by RT-PCR. **C.** Calvarial osteoblasts were isolated from *shn3*$^{+/+}$ and *shn3*$^{-/-}$ pups at postnatal day 4 and mRNA levels of *Dkk1* were measured by RT-PCR. **D.** The osteocyte line OCY454 was transduced with lentiviruses expressing control-shRNA (Sh-ctrl)- or Shn3-shRNA (Sh-shn3) and mRNA levels of *Sost* were measured by RT-PCR. Values represent mean ± SD by an unpaired two-tailed Student's t-test. ns, not significant.

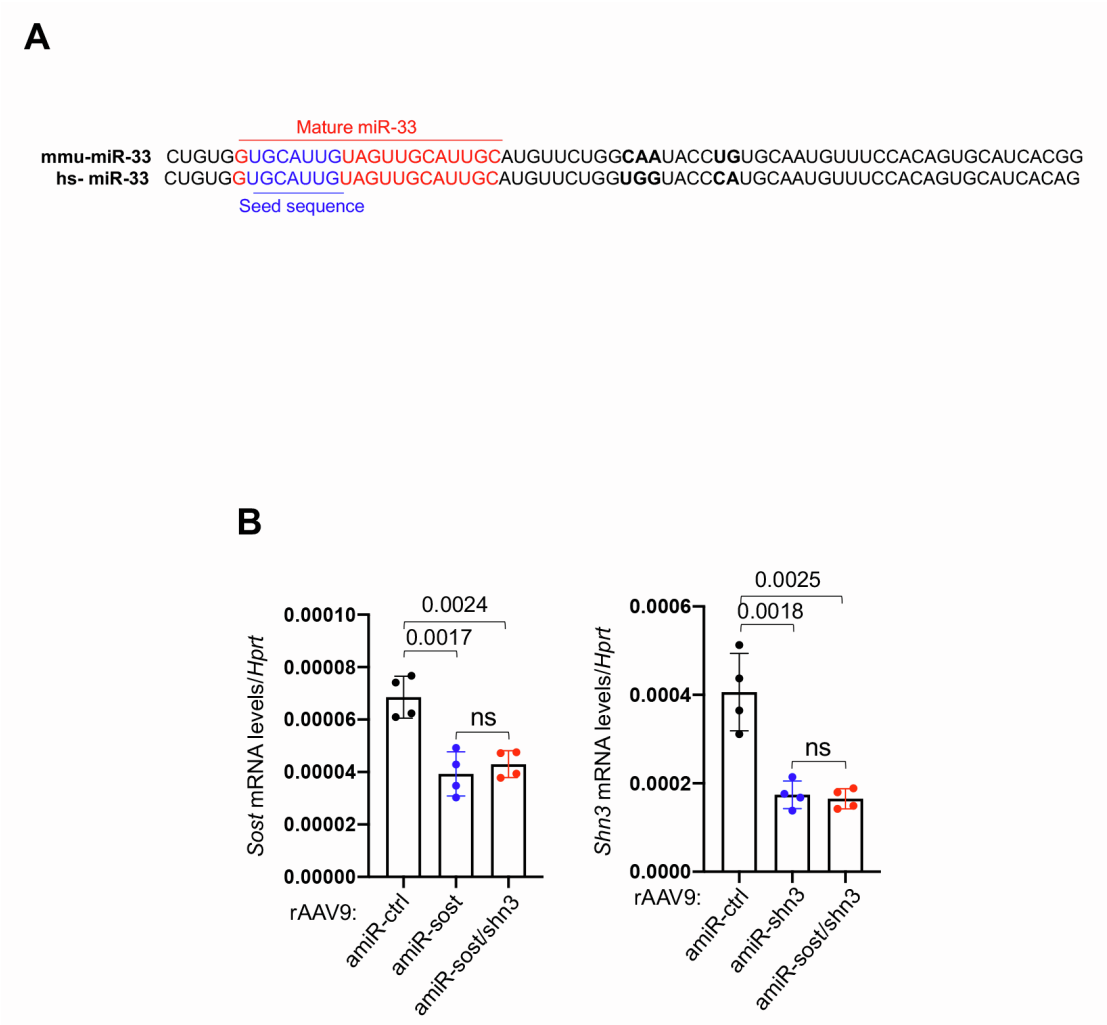

Fig. S3. Characterization of human amiR targeting mouse *Shn3*.
A. Nucleotide sequences of mouse (mmu-miR-33) and human (hs-miR-33) miR-33 that include mature and seed sequences (in blue) of miR-33. **B.** The Ocy454 osteocytic cell line was incubated with rAAV9.DSS carrying *amiR-ctrl*, *amiR-shn3*, *amiR-sost*, or *amiR-shn3/sost*, cultured under differentiation conditions for six days, and *Shn3* and *Sost* mRNA levels were measured by RT-PCR. Values represent mean ± SD by a one-way ANOVA test. ns, not significant.

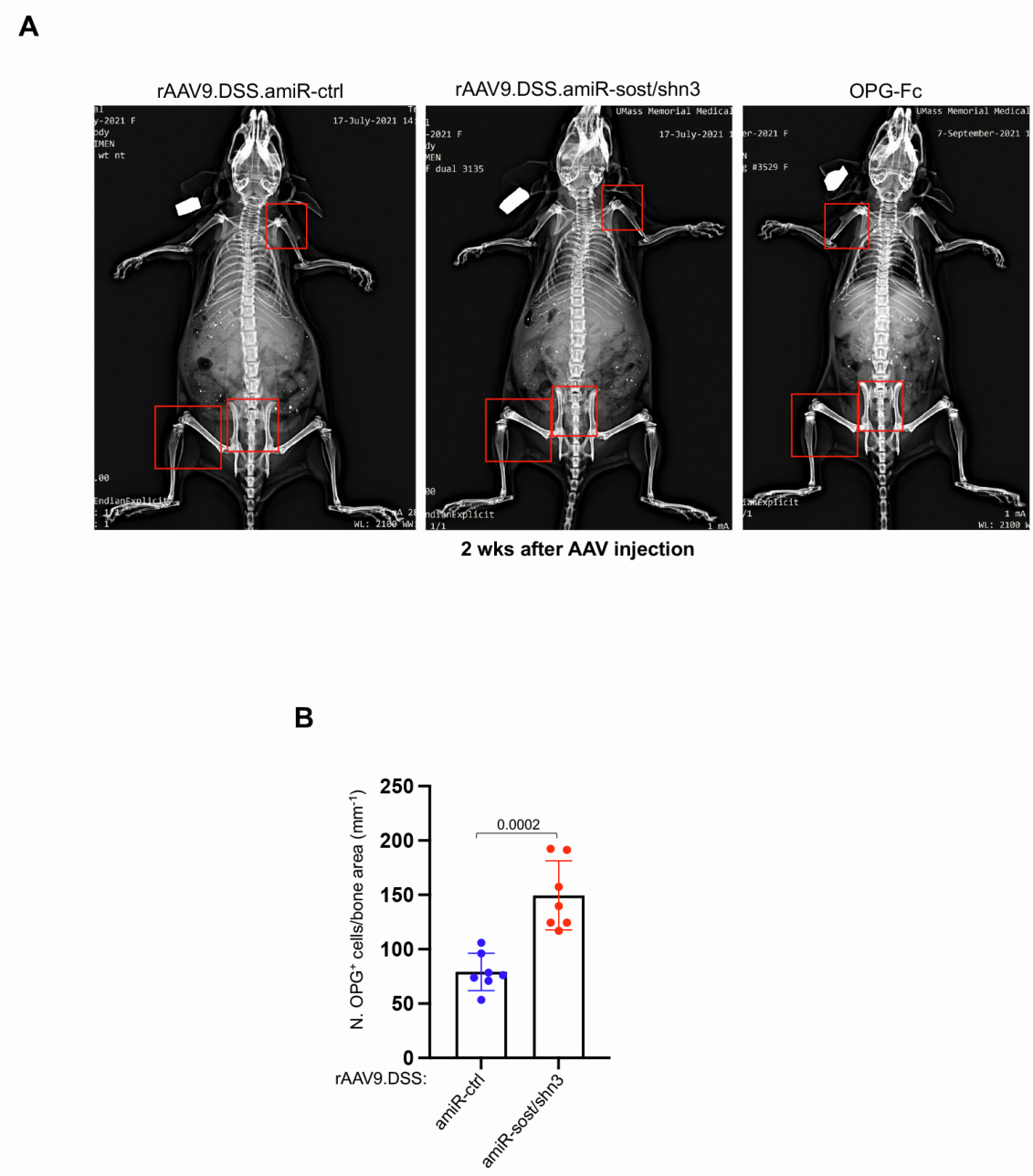

Fig. S4. Systemic delivery of WNT-modulating gene silencers increases bone accrual. **A.** One-month-old mice were treated with a single dose of rAAV9.DSS vectors carrying *amiR-ctrl* or *amiR-shn3/sost* (5 x 10^{13} vg/kg) via intravenous (i.v.) injection or with OPG-Fc (1 mg/kg) via intraperitoneal (i.p.) injection and two weeks later, bone accrual was assessed by radiography. Red boxes indicate the areas of increased bone accrual. The same experiment was performed in **Fig. 2B**. **B.** Two-month-old mice were injected i.v. with rAAV9.DSS (5 x 10^{13} vg/kg) carrying *amiR-ctrl* or *amiR-sost/shn3*, and four weeks later, immunohistochemistry for OPG was performed in AAV-treated femurs and OPG-expressing cells were quantitated (n = 7). The same experiment was performed in **Fig. 2I**. Values represent mean ± SD by a one-way ANOVA test.

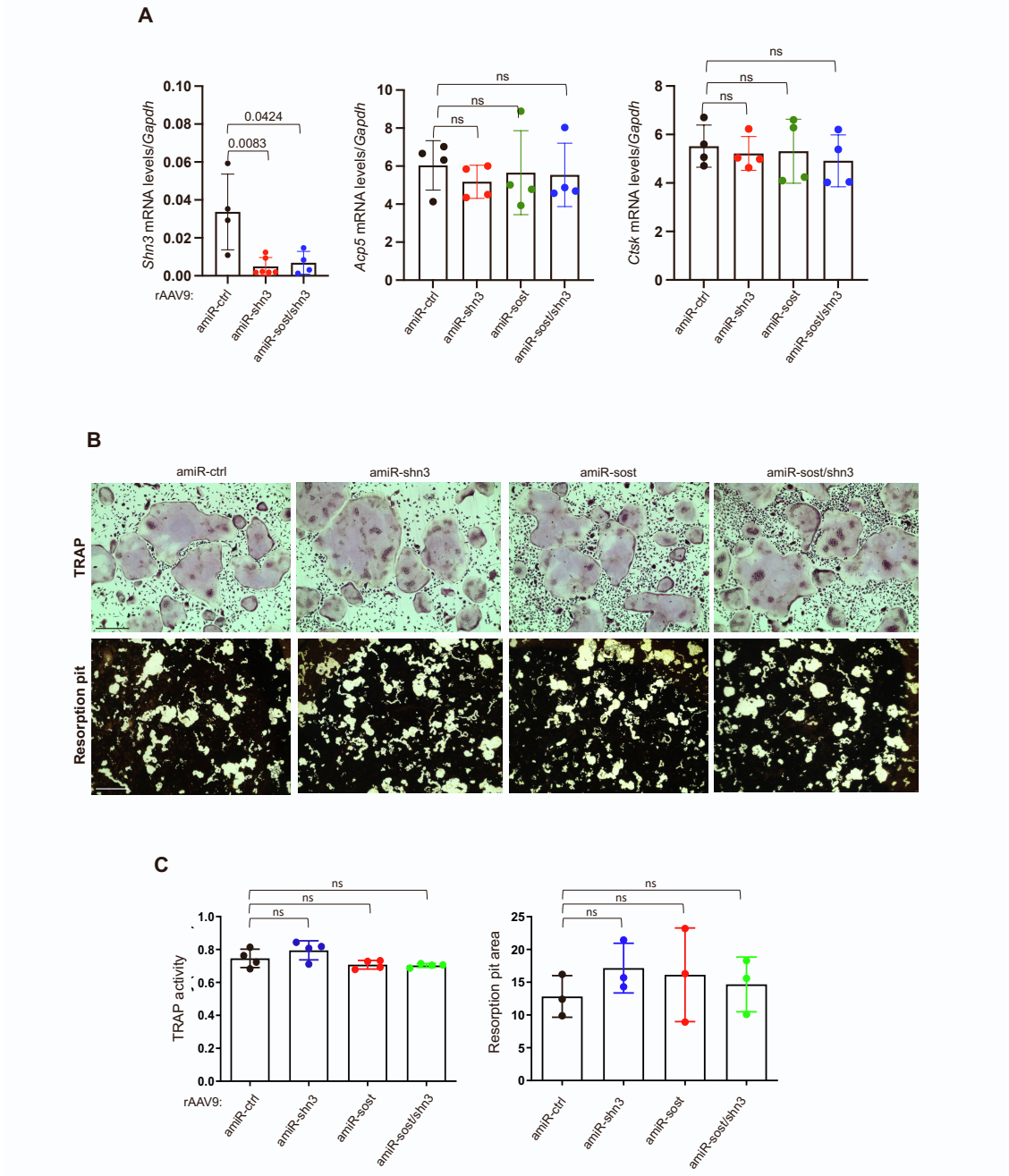

Fig. S5. Effects of WNT-modulating gene silencers on osteoclast differentiation *in vitro*. Bone marrow-derived monocytes (BMMs) harvested from 2-month-old mice were treated with M-CSF (20 ng/ml) and RANKL (10 ng/ml) for one day and then transduced with rAAV9.DSS carrying *amiR-ctrl*, *amiR-shn3*, *amiR-sost*, or *amiR-shn3/sost* (5 x 10^6 MOI). AAV-transduced BMMs were cultured with M-CSF and RANKL for six days to differentiate them into mature osteoclasts. **A.** Expression of *Shn3* and osteoclastogenic genes, *Acp5* and *Ctsk*, was assessed by RT-PCR and normalized to *Gapdh* (n = 4). *Sost* mRNAs were not detected by RT-PCR. **B, C.** Osteoclast differentiation and resorption activity were assessed by TRAP staining and resorption pit assay, respectively (n = 4). Scale bars: 1 mm. Values represent mean ± SD by a one-way ANOVA test. ns, not significant.

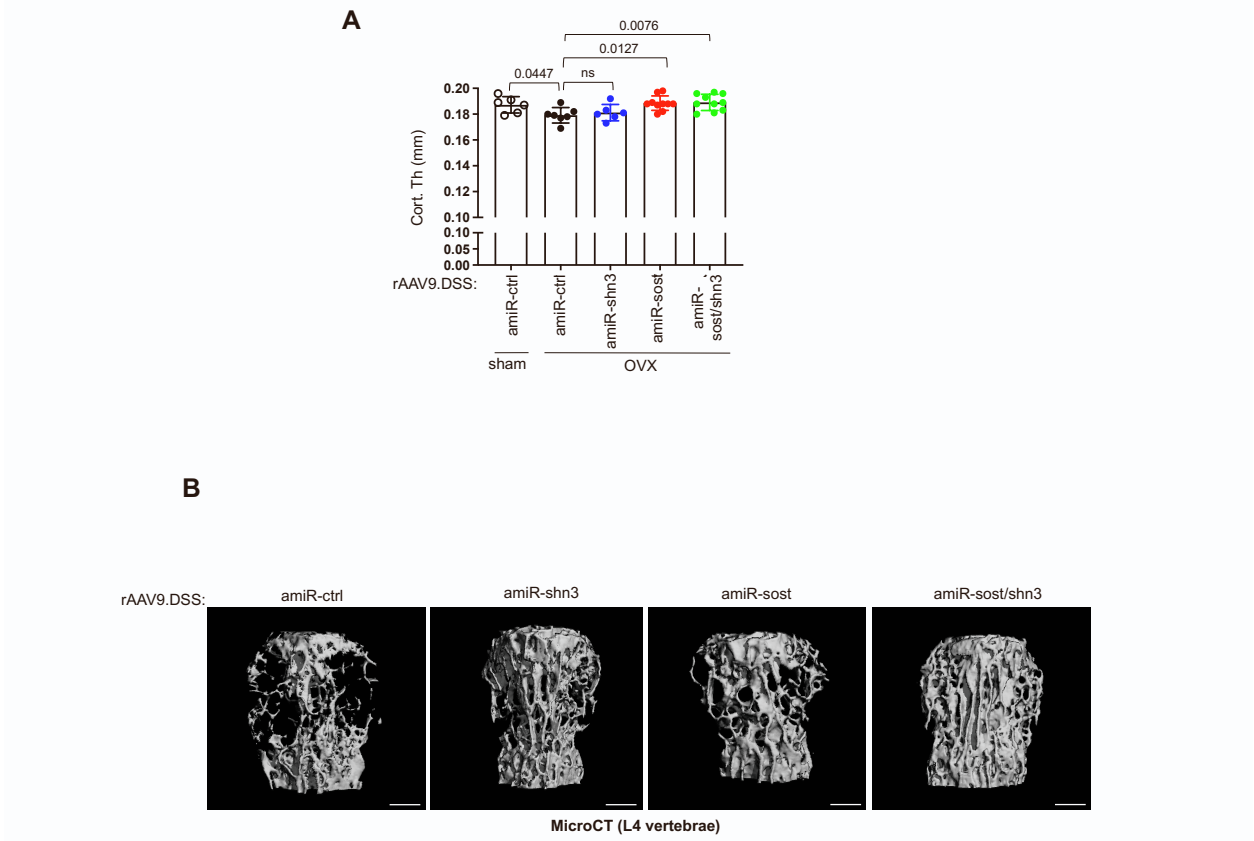

Fig. S6. Bone-targeted AAV gene silencers reverse bone loss in mouse models of osteoporosis. **A.** Sham or OVX surgery was performed on three-month-old female mice, and six weeks later, mice were injected i.v. with rAAV9.DSS (5 x 10^{13} vg/kg) carrying *amiR-ctrl*, *amiR-shn3, amiR-sost,* or *amiR-sost/shn3*. Eight weeks later, cortical thickness of AAV-treated femurs was assessed by microCT (n = 5–10). The same experiment was performed in **Fig. 3E**. **B.** 20-month-old male mice were injected i.v. with rAAV9.DSS (5 x 10^{13} vg/kg) carrying *amiR-ctrl*, *amiR-shn3, amiR-sost, or amiR-sost/shn3*, and two months later, trabecular bone mass in lumbar vertebrae (L4) was assessed by microCT. Representative 3D-reconstruction is displayed (n = 8–10). Scale bars: 500 µm. The same experiment was performed in **Fig. 3I**. Scale bars: 1 mm. Values represent mean ± SD by a one-way ANOVA test. ns, not significant.

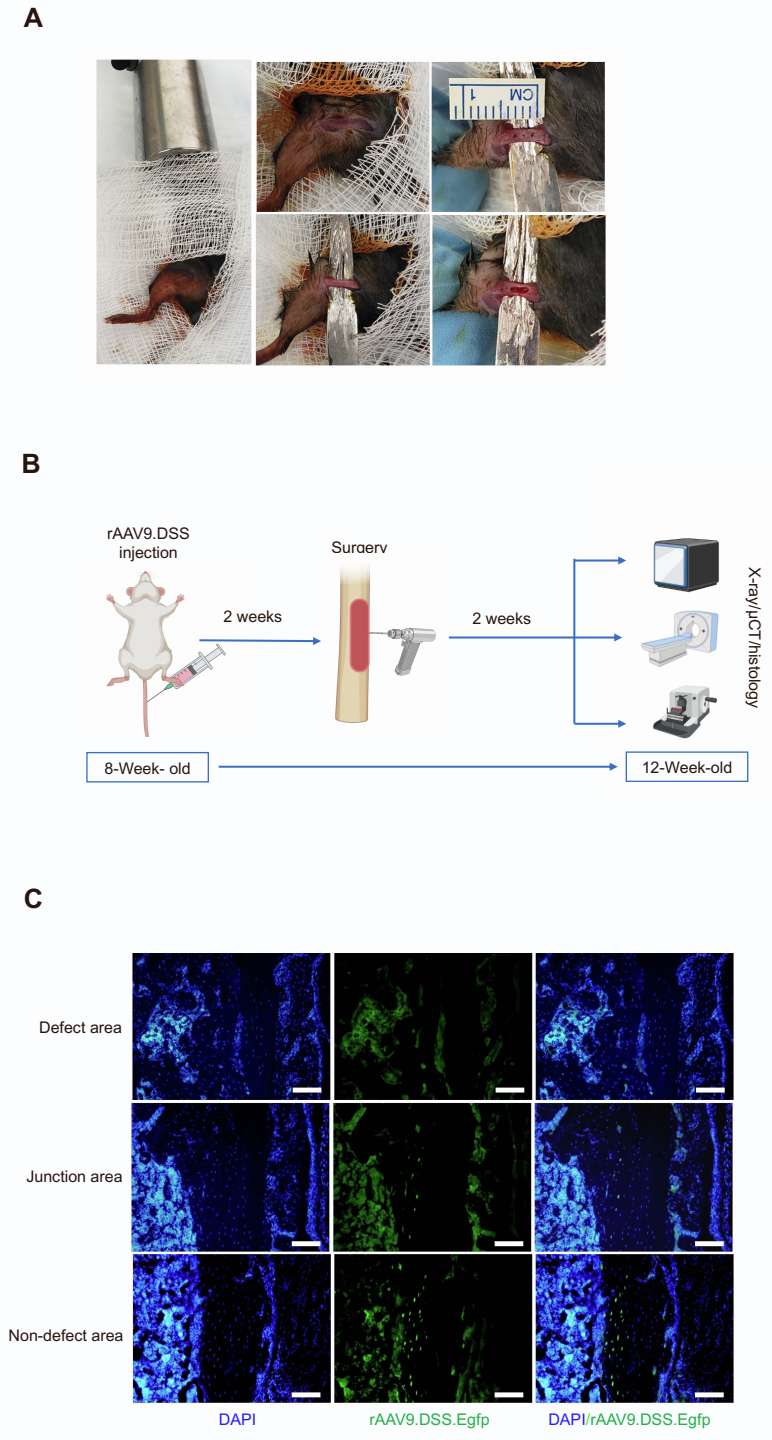

Fig. S7. Effects of WNT-modulating gene silencers on the healing of cortical bone defects. **A.** Images showing the surgical procedure of cortical bone defect in the femur. **B.** Diagram of the study and treatment methods (created with biorender.com). **C.** 8-week-old mice were i.v. injected with rAAV9.DSS.egfp (5 x 10^{13} vg/kg), and two weeks later, a 3 mm-length of cortical bone defect was generated on the lateral aspect of the left femurs. GFP expression in the cryo-sectioned femurs was visualized by fluorescence microscopy two weeks post-surgery (n=3). Scale bars: 500 μm. The same experiment was performed in **Fig. 4A**.

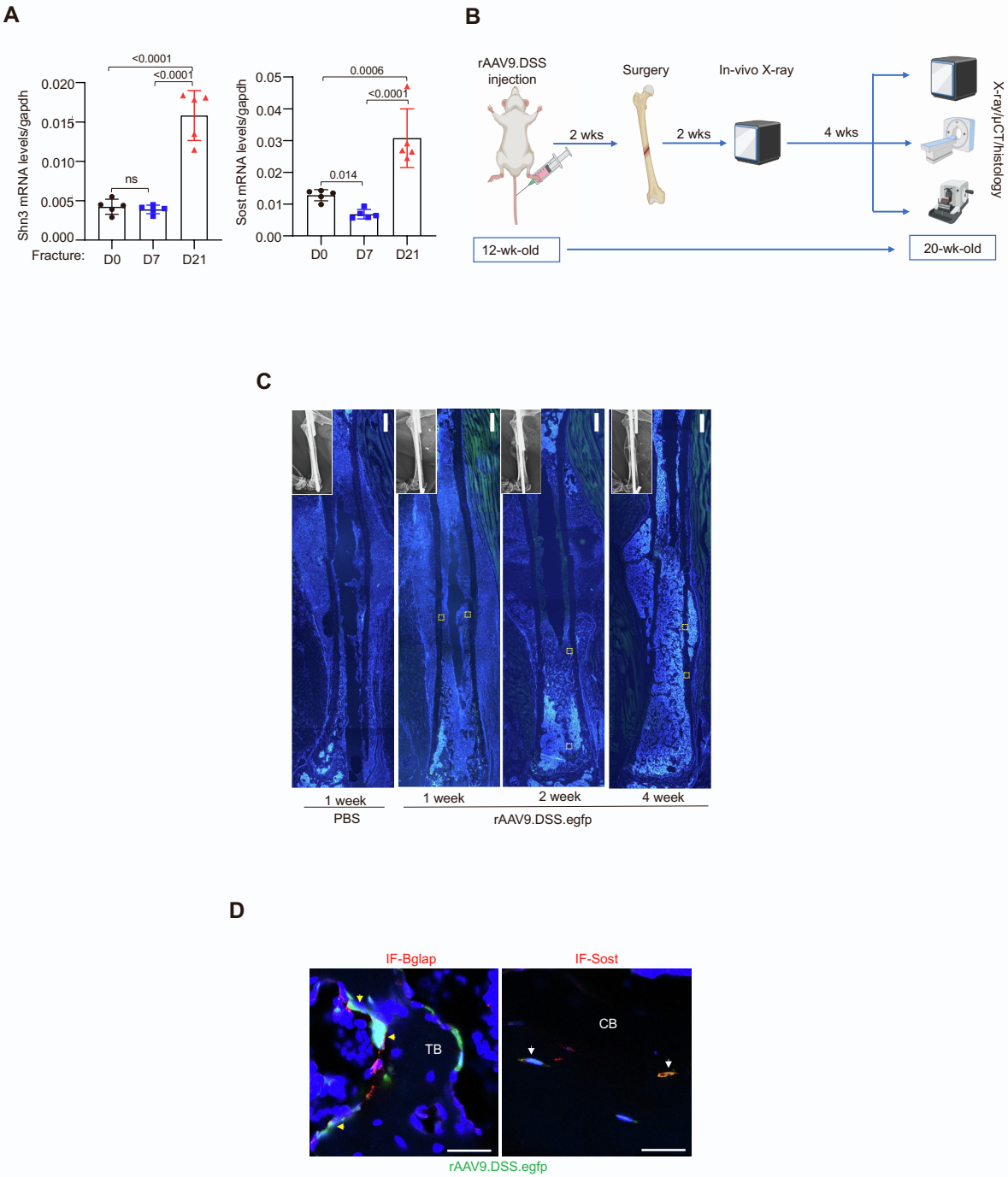
A
<0.0001
<0.0001
ns
Shn3 mRNA levels/gapdh
0.020
0.015
0.010
0.005
0.000
Fracture:
D0
D7
D21
0.0006
<0.0001
0.014
Sost mRNA levels/gapdh
0.05
0.04
0.03
0.02
0.01
0.00
D0
D7
D21
B
rAAV9.DSS injection
Surgery
In-vivo X-ray
2 wks
2 wks
4 wks
X-ray/μCT/histology
12-wk-old
20-wk-old
C
1 week
PBS
1 week
2 week
4 week
rAAV9.DSS.egfp
D
IF-Bglap
IF-Sost
TB
CB
rAAV9.DSS.egfp

Fig. S8. Systemic delivery of a bone-targeted AAV can transduce osteoblast-lineage cells at fracture sites.

A. Tissue RNA was harvested from the tibial fracture sites, and mRNA levels of *Shn3* and *Sost* were measured by RT-PCR (n=5/group). **B.** Diagram of the study and treatment methods (created with biorender.com). **C-D.** Three-month-old mice were i.v. injected with rAAV9.DSS.egfp, and two weeks later, femoral osteotomy and intramedullary fixation were performed on the left femurs. To visualize AAV-transduced cells in the fracture areas, EGFP expression in the cryo-sectioned femurs was assessed by fluorescence microscopy 1, 2, and 4 weeks postoperatively (n = 3, **C**). Alternatively, cryo-sectioned femurs were immunostained with Bglap (osteoblasts, yellow arrows) or Sost (Osteocytes, white arrows, **D**). The same experiment was performed in **Fig. 4E.** Scale bars: C, 600 μm; D, 25 μm. Values represent mean ± SD. Significance was tested with a one-way ANOVA test. ns, not significant.

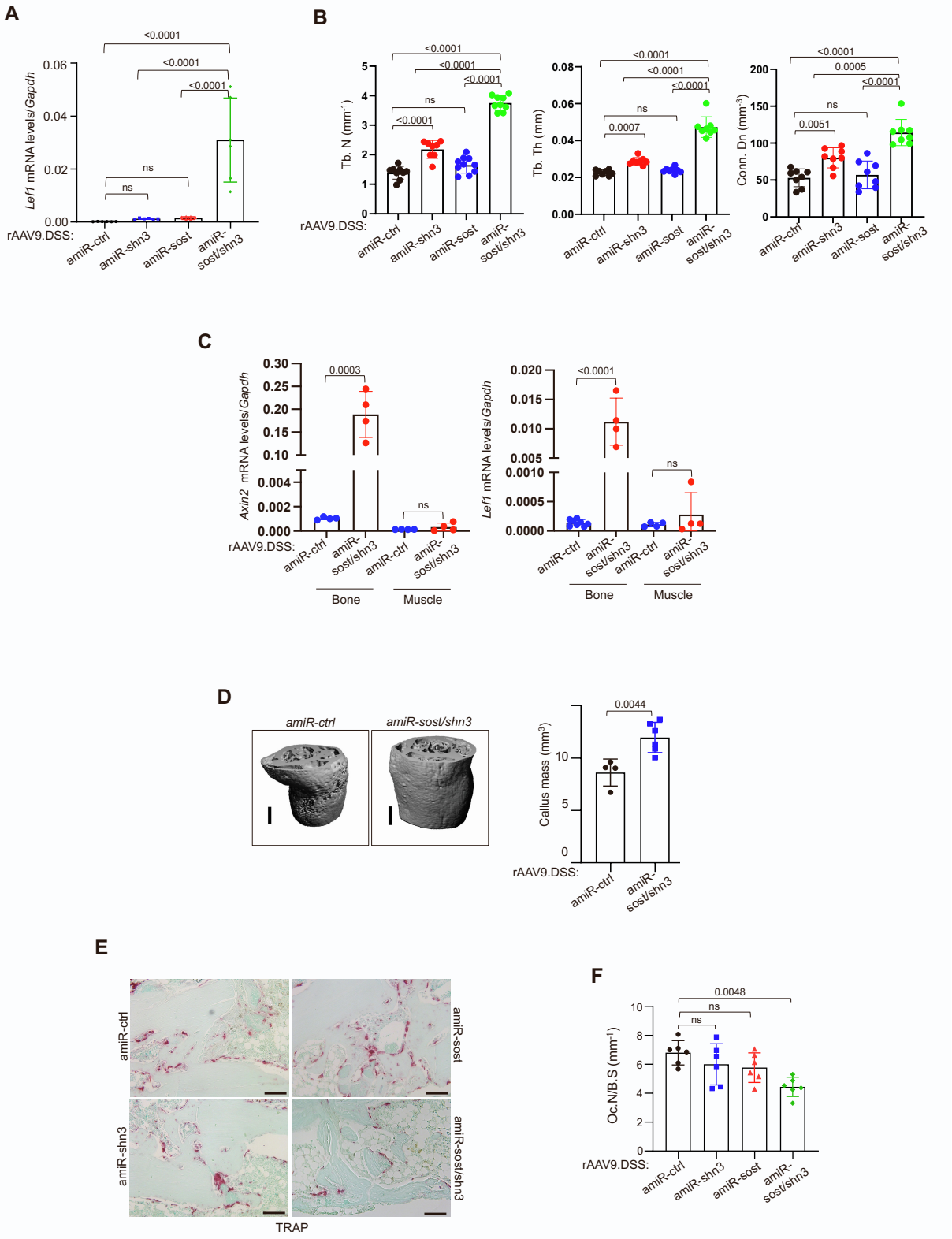
A
Lef1 mRNA levels/Gapdh
<0.0001
<0.0001
<0.0001
ns
ns
rAAV9.DSS:
amiR-ctrl
amiR-shn3
amiR-sost
amiR-sost/shn3
B
Tb. N (mm-1)
Tb. Th (mm)
Conm. Dn (mm-3)
0.0007
0.0005
0.0051
C
Axin2 mRNA levels/Gapdh
Lef1 mRNA levels/Gapdh
0.0003
Bone
Muscle
D
amiR-ctrl
amiR-sost/shn3
Callus mass (mm3)
0.0044
E
TRAP
F
Oc.N/B.S (mm-1)
0.0048

Fig. S9. Effects of WNT-modulating gene silencers on bone fracture healing.
Three-month-old mice were i.v. injected with rAAV9.DSS carrying *amiR-ctrl*, *amiR-shn3, amiR-sost,* or *amiR-sost/shn3*, and two weeks later, femoral osteotomy and intramedullary fixation were performed on the left femurs. mRNA levels of the β-catenin target gene *Lef1* in RNA from the contralateral tibia **(A)** or the skeletal muscle of the fractured femurs **(C)** were measured six weeks post-fracture (n = 8). The same experiment was performed in **Fig. 4G,** but for Axin2 mRNA. Trabecular bone mass of contralateral femurs without the surgery (**B)** and callus bone mass in the fractured sites (**D)** were assessed by microCT (n = 8). Fractured sites of AAV-treated femurs were stained for TRAP and TRAP-stained osteoclasts were quantitated (n =6, **E, F**). Tb.N: trabecular bone number, Tb.Th: trabecular bone thickness, Conn.D: connective density. Oc.N/B.S: osteoclast number/bone surface. Scale bar: D, 1 mm; E, 100 μm. Values represent mean ± SD by a one-way ANOVA test. ns, not significant.

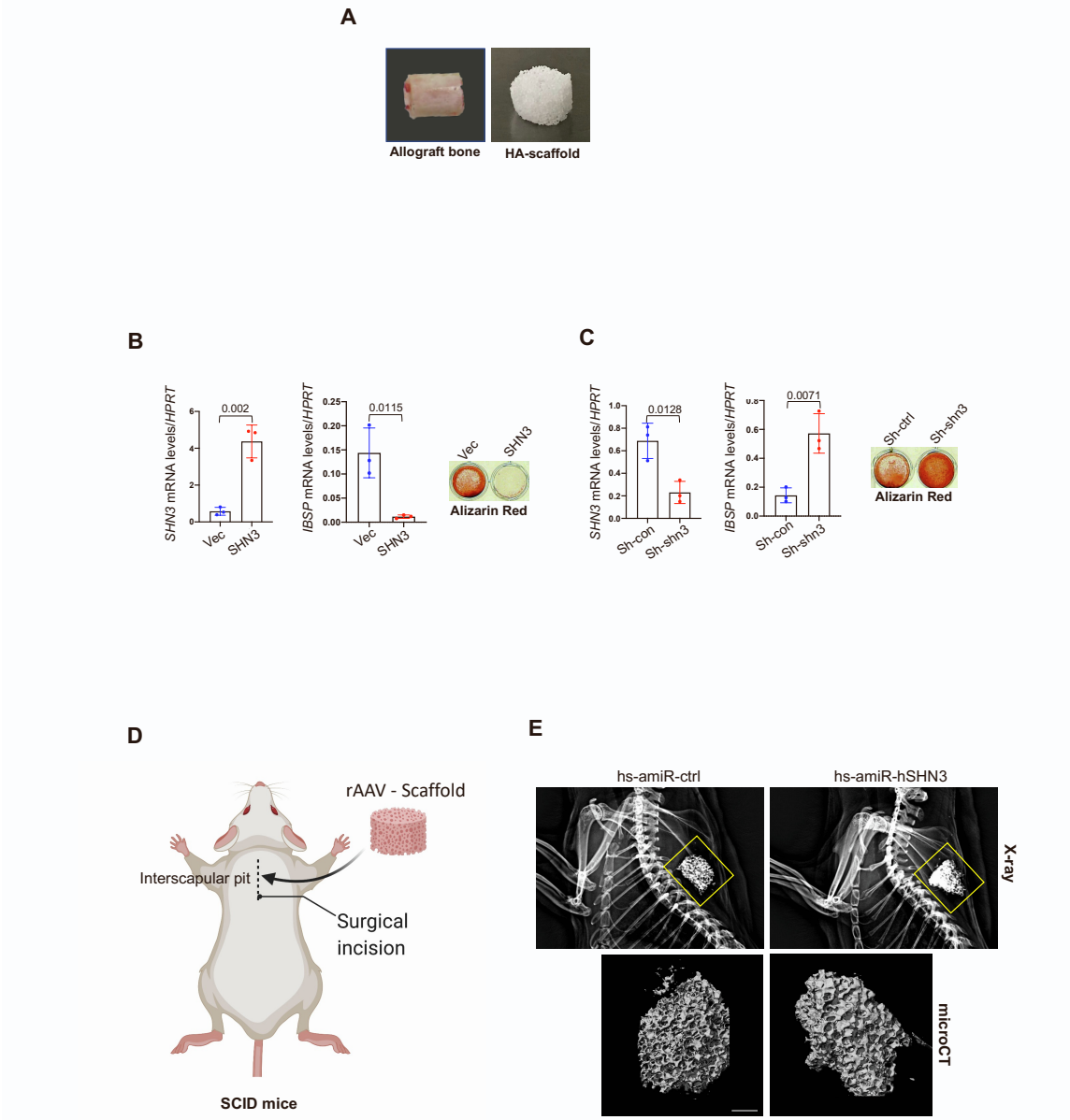

Fig. S10. Generation of a human skeletal organoid in xenograft mice.
A. Representative pictures showing mouse decellularized bone graft and hydroxyapatite (HA)-based scaffold. **B, C.** Human BMSCs were transduced with lentiviruses expressing vector control (Vec), mouse SHN3 (1-3557 aa, **B**), control-shRNA (Sh-con), or Shn3-shRNA (Sh-shn3, **C**), cultured under osteogenic conditions, and mRNA levels of *SHN3* and *IBSP* were measured by RT-PCR. Alternatively, mineralization deposit was assessed by alizarin red staining (n=3). **D, E.** Diagram showing a surgery procedure to implant a human skeletal organoid into the interscapular fat pad of immunodeficient SCID mice (created with biorender.com) **(D)**. The HA-scaffold was incubated with rAAV9.DSS carrying *hs-amiR-ctrl or hs-amiR-hSHN3* for one hour, and then human BMSCs were cultured on the AAV-treated scaffold under osteogenic conditions for two days. The treated scaffold was implanted into the interscapular fat pads, and four weeks later, bone formation was assessed by radiography **(E, top)** and microCT (**E, bottom**, n=5). Values represent mean ± SD by an unpaired two-tailed Student's t-test.

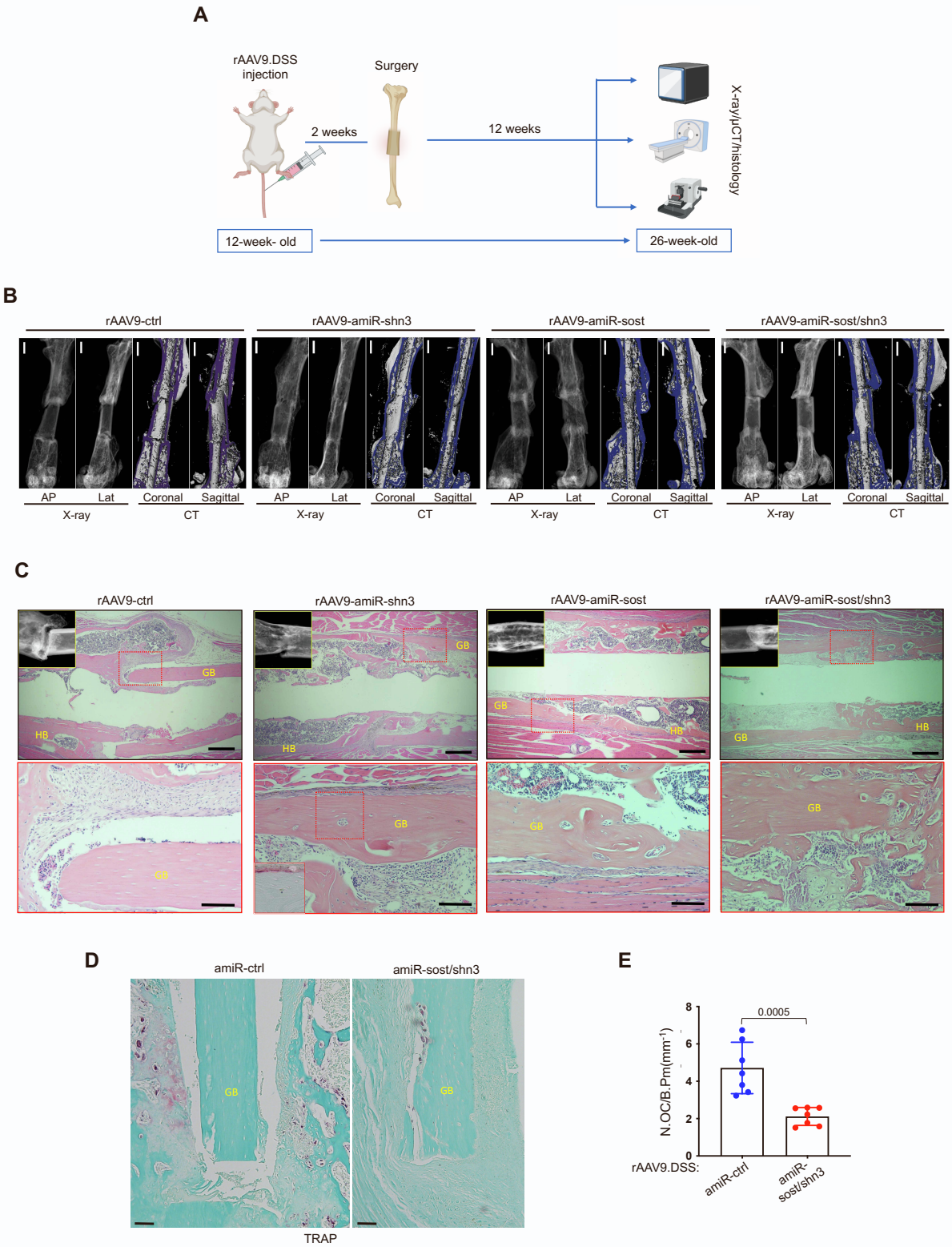
A
rAAV9.DSS injection
Surgery
2 weeks
12 weeks
X-ray/μCT/histology
12-week- old
26-week-old
B
rAAV9-ctrl
rAAV9-amiR-shn3
rAAV9-amiR-sost
rAAV9-amiR-sost/shn3
AP
Lat
Coronal
Sagittal
X-ray
CT
C
rAAV9-ctrl
rAAV9-amiR-shn3
rAAV9-amiR-sost
rAAV9-amiR-sost/shn3
GB
HB
D
amiR-ctrl
amiR-sost/shn3
TRAP
E
0.0005
N.OC/B.Pm(mm-1)
rAAV9.DSS:
amiR-ctrl
amiR-sost/shn3

Fig. S11. Therapeutic effects of systemically delivered WNT-modulating gene silencers on critical-sized bone defect

A. Diagram of the study and treatment methods (created with biorender.com). **B-E.** Three-month-old mice were i.v. injected with rAAV9.DSS (5 x 10^{13} vg/kg) carrying *amiR-ctrl, amiR-shn3*, *amiR-sost,* or *amiR-sost/shn3*, and two weeks later, decellularized isograft was implanted into the osteotomy site of the left femurs. Twelve weeks later, radiography, microCT, and H&E staining were performed on the injured femurs to assess the rate of osseous union between the implanted isograft to the host bone. (n = 5–6, **B, C**). HB: host bone, GB: graft bone. The same experiment was performed in **Fig. 6A and B**. Alternatively, the injured femurs were stained for TRAP and TRAP-stained osteoclasts were quantitated (n = 7, **D, E**). Scale bars: B, 1 mm; C, top, 400 μm; C bottom, D, 100 μm. Values represent mean ± SD by an unpaired two-tailed Student's t-test.

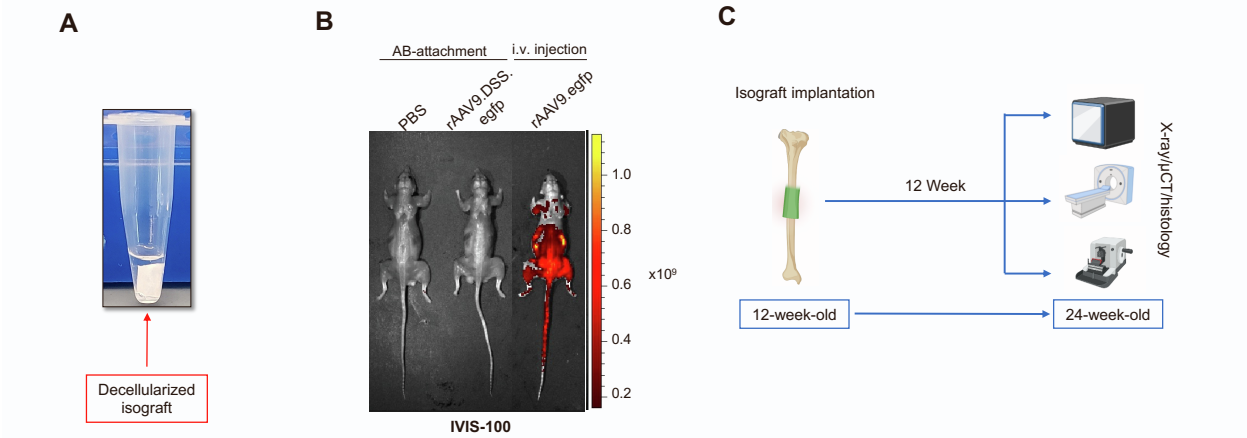

Fig. S12. Transplantation of the isograft carrying WNT-modulating gene silencers to the osteotomy sites in a mouse model of critical-sized bone defect

A. Preparation of decellularized isograft attached with rAAV9.DSS. Decellularized isograft was incubated with rAAV9.DSS (2.5 x 10^{11} GC) for one hour. **B.** PBS-treated or rAAV9.DSS.*egfp*-attached isograft was implanted into the osteotomy site of left femurs in 3-month-old mice, and three weeks later, EGFP expression in whole body was monitored by IVIS-100 optical imaging. For systemic delivery, rAAV9.DSS.*egfp* (5 x 10^{13} vg/kg) was i.v. injected into mice (n = 3). The same experiment was performed in **Fig. 6C**. **C.** Diagram of the study and treatment methods (created with biorender.com).

Tables S1-S2

Table S1

	amiR-ctrl	amiR-shn3	amiR-sost	amiR-shn3/sost
WNT signaling threshold	weak	intermediate	intermediate	strong
Osteogenesis	no effect	mild increase	mild increase	strong increase and wane over time
Osteoclastogenesis	no effect	no effect	mild decrease	strong decrease by OPG
Bone accrual	no effect	mild increase	mild increase	strong increase
Early bone regeneration	no effect	increase	increase	increase
Osteoporosis	no effect	complete reversal	partial reversal	complete reversal
Bone fracture healing	no effect	increase	increase	little to mild increase
Critical-sized bone defect healing	no effect	increase	increase	no effect

Table S2

Gene	Forward	Reverse
Human *Shn3*	GCCCTATGTGTGCAAGCACTGT	AGTCCTGGAACAGGTCGTCACT
Mouse *Shn3*	AGAGGCCATTCAGACGAGTGT	CTGCGGAAGCTGAGAGATGT
Mouse *Gapdh*	ACTGAGCAAGAGAGGCCCTA	TATGGGGGTCTGGGATGGAA
Mouse *Actb*	AGGGAAATCGTGCGTGACAT	GAACCGCTCGTTGCCAATAG
Mouse *Lef1*	CCAAGCAAGGCATGTCCAGACACC	GCCTGACAGTGAGGATGGGTAGGG
Mouse *Dkk1*	ATCTGTCTGGCTTGCCGAAAGC	GAGGAAAATGGCTGTGGTCAGAG
Human *BGLAP*	AGAGTCCAGCAAAGGTGCAG	TCAGCCAACTCGTCACAGTC
Human *IBSP*	CAACAGCACAGAGGCAGAAA	TTGTGGTGGGGTTGTAGGTT
Mouse *Axin2*	GCAGATGAACCTGAAGGATACC	TTGATGCCATCTCGTATGTAGG
Mouse *Sost*	CTTCAGGAATGATGCCACAGAGGT	ATCTTTGGCGTCATAGGGATGGTG
Mouse *Hprt*	CTGGTGAAAAGGACCTCTCGAAG	CCAGTTTCACTAATGACACAAACG
Human *HPRT*	GCTATAAATTCTTTGCTGACCTGCTG	AATTACTTTTATGTCCCCTGTTGACTGG
EGFP	AGCAAAGACCCCAACGAGAA	GGCGGCGGTCACGAA
EGFP-probe	6FAM-CGCGATCACATGGTCCTGCTGG-TAMRA	
$(AspSerSer)_6$	GATTCATCAGATTCTTCTGATTCATCCGACTCTTCTGACAGTTCAGACAGCTCT	
$(Asp)_{14}$	GATGATGATGATGATGATGATGATGATGATGATGATGAT	
amiR-33-ctrl (*amiR-ctrl*)	tttgtcttttatttcaggtcccagatctagggctctgcgtttgctccaggtagtccgctgctcccttgggcctgggcccactgacagc cctggtgcctctggccggctgcacacctcctggcgggcagctgtgttactgtaggatcgagagggatgttctggcaatacctgtc cctctccttactacagtaacacggaggcctgccctgactgcccacggtgccgtggccaaagaggatctaagggcaccgctgag ggcctacctaaccatcgtggggaataaggacagtgtcacccctgcaggggatccggtggtggtgcaaatca	
Human amiR-33-mouse shn3 (hs-*amiR-shn3*)	gatctggcagccttggagtgggttcctgccccctcgggcacacaaacagagctgaagaccaccctgggcacctccttggctgg ccgcatacctcctggcgggcagctgtgtacaaactacttgagagcaggtgttctggtggtacccacctgctctgtaatagtttgta cacagaggcctgcctggccctcgagagactgccctgactgaaggccctatcaggtgggggaggggatcctgatagagggca ctgctgccactgttggggcccaagctgca	
amiR-33-mouse shn3 (*amiR-shn3*)	tttgtcttttatttcaggtcccagatctagggctctgcgtttgctccaggtagtccgctgctcccttgggcctgggcccactgacagc cctggtgcctctggccggctgcacacctcctggcgggcagctgtgtacaaactacttgagagcaggtgttctggcaatacctgc ctgctctgtaatagtttgtacacggaggcctgccctgactgcccacggtgccgtggccaaagaggatctaagggcaccgctga gggcctacctaaccatcgtggggaataagg acagtgtcacccctgcaggggatccggtggtggtgcaaatca	
amiR-33-human shn3 (*amiR-hshn3*)	gtcttttatttcaggtcccagatcttagggctctgcgtttgctccaggtagtccgctgctcccttgggcctgggcccactgacagcc ctggtgcctctggccggctgcacacctcctggcgggcagctgtgtttccatggtaagttcaaggctgttctggcaatacctggcct tgaagatgccatggaaacacggaggcctgccctgactgcccacggtgccgtggccaaagaggatctaagggcaccgctgag ggcctacctaaccatcgtggggaataaggacagtgtcacccccctgcaggggatccggtggtggtgcaaat	
amiR-33-mouse sost (*amiR-sost*)	gatctagggctctgcgtttgctccaggtagtccgctgctcccttgggcctgggcccactgacagccctggtgcctctggccggct gcacacctcctggcgggcagctgtgtgacctctgtggcatcattcctgttctggcaatacctgggaatgatcgcgcagaggtcac acggaggcctgccctgactgcccacggtgccgtggccaaagaggatctaagggcaccgctgagggcctacctaaccatcgt ggggaataaggacagtgtcacccctgca	
amiR-33-mouse sost (*amiR-sost*) +	gatctagggctctgcgtttgctccaggtagtccgctgctcccttgggcctgggcccactgacagccctggtgcctctggccggct gcacacctcctggcgggcagctgtgtgacctctgtggcatcattcctgttctggcaatacctgggaatgatcgcgcagaggtcac	

human amiR-33 -mouse shn3 (hs-*amiR-shn3*)	acggaggcctgccctgactgcccacggtgccgtggccaaagaggatctaagggcaccgctgagggcctacctaaccatcgt ggggaataaggacagtgtcacccctgcaggggatccggtggtggtgcaaatcaaagaactgctcctcagtggatgttgccttta cttctaggcctgtacggaagtgttacttctgctctaaaagctgcggaattgtacccgcggccgatccaccggtcgccaccatggg gcagccttggagtgggttcctgccccctcgggcacacaaacagagctgaagaccaccctgggcacctccttggctggccgca tacctcctggcgggcagctgtgtacaaactacttgagagcaggtgttctggtggtacccacctgctctgtaatagtttgtacacag aggcctgcctggccctcgagagactgccctgactgaaggccctatcaggtgggggaggggatcctgatagagggcactgctg ccactgttggggcccaagaagct
Human amiR-33-human shn3-1 (hs-*amiR-hshn3-1*)	ggcagccttggagtgggttcctgccccctcgggcacacaaacagagctgaagaccaccctgggcacctccttggctggccgc atacctcctggcgggcagctgtgtttccatggtaagttcaaggctgttctggtggtacccagccttgaagatgccatggaaacac agaggcctgcctggccctcgagagactgccctgactgaaggccctatcaggtgggggaggggatcctgatagagggcactg ctgccactgttggggcccaag
Human amiR-33-human shn3-2 (hs-*amiR-hshn3-2*)	ggcagccttggagtgggttcctgccccctcgggcacacaaacagagctgaagaccaccctgggcacctccttggctggccgc atacctcctggcgggcagctgtgtccatggtaagttcaaggctgtgttctggtggtacccacagccttgttcctaccatggacaca gaggcctgcctggccctcgagagactgccctgactgaaggccctatcaggtgggggaggggatcctgatagagggcactgct gccactgttggggcccaag
Human SHN3 shR	ccgggccttgaacttaccatggaaactcgagtttccatggtaagttcaaggctttt